ANALYSIS OF MAGNETOHYDRODYNAMIC HEAT AND MASS TRANSFER WITH CARBON NANOTUBES-GRAPHENE CASSON HYBRID NANOFLUID

Juma Belindar Atieno (B.Ed)

I56/20185/2020

A research project submitted in partial fulfilment of the requirements for the award of the degree of Masters of Science (Applied Mathematics) in the School of Pure and Applied Sciences of Kenyatta University

NOVEMBER 2022

Declaration

Declaration by the Candidate

This project is my original work and has not been submitted for any award of a degree in any University.

Name: Belindar Atieno Juma

Signature: .....

Date: .....

Declaration by the Supervisor

This project has been submitted for examination with my approval as the University

Name: Dr. W. N. Mutuku

Signature: .....

Date: .....

Department of Mathematics and Actuarial Science, Kenyatta University.

Acknowledgement

I convey my immense gratitude to God, for granting me the capacity to reach this far in my research work. I appreciate my supervisor, Dr. Winifred Mutuku, and research mentor, Dr Abayomi S. Oke, whose assistance in the project development has been invaluable. Special appreciation to my mother, Rose Anyango, for the unrelenting support. To all my lecturers who taught and interacted with me during my MSc program, I appreciate all your help and encouragement. This work came to fruition because of all of your continuous assistance.

Abstract

Fluids such as liquids and gases are amassed into either Newtonian or non-Newtonian groups. Most fluids fall under the non-Newtonian category and, as a result, various models like Casson fluid and Williamson fluid model have been proposed to deal with the non-Newtonian fluid behaviour. Due to its ability to model the flow of blood, Casson fluid model is of major medical importance. A development on ordinary fluids are nanofluids, which posses enhanced thermophysical properties. Hybrid nanofluid, obtained when two non-identical nanoparticles are dispersed in a fluid, is an improvement on the novel nanofluids. It has superior thermal conductivity when compared with nanofluids or ordinary fluids. Multiple research have shown that the shape of the nanoparticles used during the hybridization process has significant impact on the thermal properties of the hybrid formed. Applications of hybrid nanofluid include refrigerators, electronic devices, and cancer treatments. In the study of hybrid nanofluids, the focus has been placed on the dynamic properties and heat transfer rate. In consensus, the superiority of the hybrid's properties are emphasized. Carbon being the most abundant product, hardest, strongest and stable known compound, it is an excellent thermal conductor. CNTs and graphene are allotropes of Carbon. In the HAMT research, no researcher has explored the impact of suspending a combination of CNTs and graphene nanoparticles on a Casson base fluid. To bridge this gap, this study is designed to analyse the HAMT rate of a 2-D magnetohydrodynamic hybrid Casson nanofluid. The nanoparticles are Carbon nanotubes and Graphene. The flow is across a surface stretching exponentially. Volume fraction, nanoparticle size and other pertinent parameters are investigated on the HAMT rate.The governing equations are converted to their non - dimensional form using similarity variables, and subsequently to an ODEs. The RK4 with Shooting Technique is adopted as a method of solution. Simulation of the model and investigation of the HAMT rate is carried out using MATLAB bvp4c. The primary velocity is reduced with Casson fluid parameter but enhanced with the radiation parameter. The temperature profiles boost with Casson fluid parameter, magnetic and radiation parameters. The local skin friction increases with Casson fluid parameter and radiation parameter but decreases with magnetic field strength. HAMT rate is enhanced with increasing Grashof number but decreases with Casson fluid parameter and magnetic field strength.

Contents

Nomenclature

Variables and parameters	
u, v Velocity along x, y-axes	τ_w Shear stress
T Hybrid nanofluid temperature	C_f Skin friction coefficient
T_w Temperature at the wall	q Radiation heat flux
T_∞ Temperature at free stream	q_w Surface heat flux
C Hybrid nanofluid concentration	L Characteristic length
C_w Concentration at the wall	ϕ Volume fraction
C_∞ Concentration at free stream	Pr Prandtl number
ν Kinematic viscosity coefficient	Gr Grashof number
μ Dynamic viscosity coefficient	Re Reynold number
ρ Density coefficient	Sh Sherwood number
β Thermal expansion coefficient	Nu Nusselt number
σ Electric conductivity coefficient	Sc Schmidt number
g^* Acceleration due to gravity	λ Velocity parameter
B_0 Magnetic field strength	M Magnetic parameter
c_p Specific heat capacity	γ Casson fluid parameter
α Thermal diffusivity	R Radiation parameter
D_T Thermophoretic diffusivity	N_b Brownian motion parameter
D_B Brownian diffusivity	N_t Thermophoretic parameter
K Thermal conductivity	K^* Mean absorption coefficient
σ^* Stefan-Boltzman constant	

subscripts	**meaning**
hnf	hybrid nanofluid
1	CNT nanofluid
2	graphene nanofluid
f	Casson fluid

List of Acronyms

Acronym	*Meaning*
HAMT	Heat and mass transfer
CNTs	Carbon nanotubes
SWCNTs	Single wall carbon nanotubes
ESS	Exponentially stretching surface
MHD	Magnetohydrodynamics
2-D	Two Dimensional
BC	Boundary condition
IC	Initial Condition

List of Figures

List of Tables

Chapter 1

Introduction

1.1 Background

Fluids are non-solid states of matter and are broadly considered as either Newtonian or non-Newtonian fluids. Newtonian fluids relate the shear stress and shear strain rate linearly; examples include water and air. The fact that there are very few fluids that can be classified as Newtonian fluids, most of the natural and engineered fluids fall in the non-Newtonian category. The non-Newtonian fluids lack the simple linear relation between the shear stress and shear strain rate. Tomato paste, clay suspension, and crude oils are examples of non-Newtonian fluids. Models proposed to deal with different non-Newtonian fluids include models of Casson fluid and Williamson fluid. The equation that describes the Casson fluid is of major medical importance due to its ability to model the flow of blood as demonstrated by Blair (1959) and Venkatesan *et al.* (2013). Unfortunately, the low thermal conductivities of most known fluids have limited their applicability in several industrial processes.

The search for thermally conducting fluids with better qualities prompted Maxwell (1873) to suggest adding small millimetre-scale solid particles to a fluid. To establish the validity of the proposal, several deterministic experiments were conducted and it was deduced that the heterogeneous solid-fluid mixture possessed better thermal and electrical qualities compared to the ordinary fluid. Despite the groundbreaking advancement in the history of fluid engineering, a major setback was birthed. The solid particles would settle after a short duration and this often resulted in clogging and corrosion of the pipes. The emergence of nanotechnology prompted a refinement

of Maxwell's work by Choi and Eastman (1995). They proposed that the millimetre-sized solid particles should be replaced with nanometre-sized solid particles. The nanometre-sized particles used were later called nanoparticles and the fluid in which the nanoparticles are suspended was called the base fluid. The resulting nanoparticles suspension in a base fluid is now called nanofluids. Meanwhile, experiments showed that using smaller solid particles than the nanoparticles resulted in clumping and reduced the thermal conductivity rate of the nanofluids. Some other experiments have shown that the nanoparticle shape has significant effects on the thermal property of the nanofluid. Research done by Elias *et al.* (2013) shows that cylindrically shaped nanoparticles have better thermal conductivity than other differently shaped nanoparticles such as spherically shaped and blade-shaped nanoparticles. The nanoparticles can be classified as shown in the figure below.

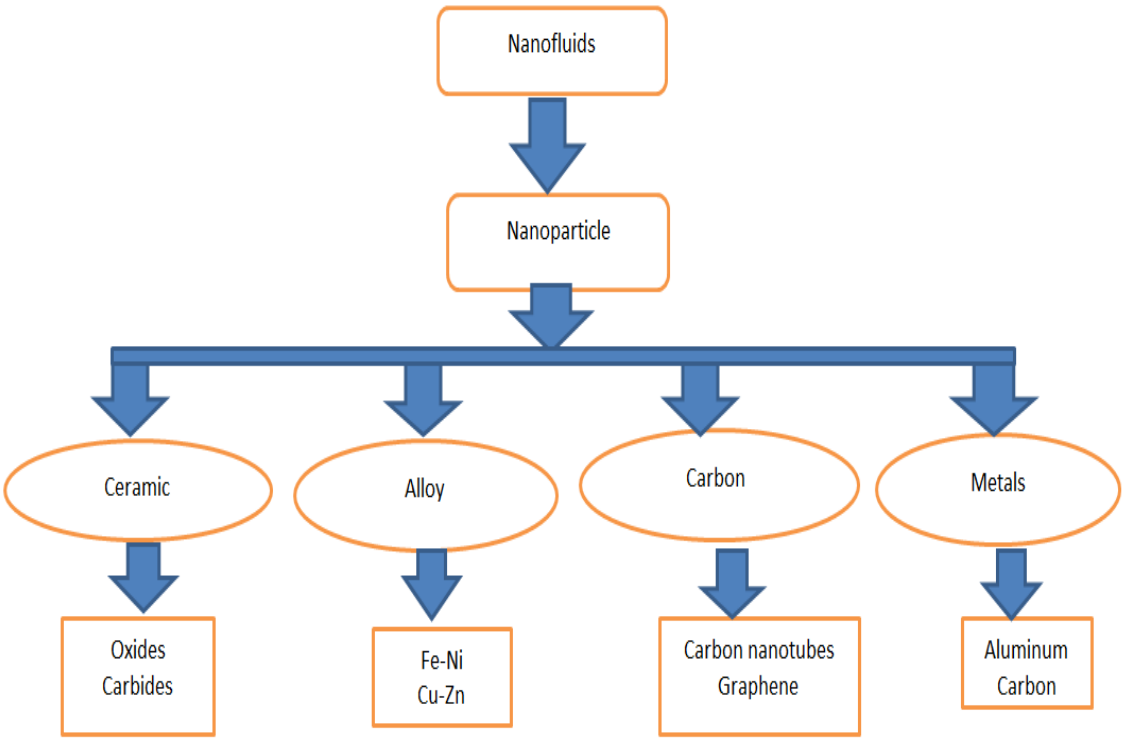

Figure 1.1: Classification of nanoparticles

The nanofluids have found their way into different areas of application due to their enhanced heat transfer rate. They are used in cooling electrical, industrial, and automotive devices, in nuclear reactors, and in the biomedical field. Due to this vast range of applications, the curiosity of whether there exists a better thermally conducting fluid was sparked. Scientists researched various ways of improving thermal conductivity in nanofluids. Suresh *et al.* (2011) discovered a new class of fluid called hybrid nanofluids. This opened a completely new field of fluid study. Researchers like Hayat and Nadeem (2017), Subhani and Nadeem (2018), Sheikholeslami *et al.* (2019), Waini *et al.* (2019), Tassaddiq *et al.* (2020), and Othman *et al.* (2021) started to build the knowledge base in this field. Their research is discussed further in the literature review.

Alfvén (1942) discovered a science dealing with the investigation of the behaviour of electrically conducting fluid as it passes through a magnetic field. He called this science magnetohydrodynamics (MHD). This branch of fluid mechanics gained attention due to its application in many industrial processes, like bioreactors, electricity generation, and design of the electro-magnetic pumps and flowmeters. This research work is focused on MHD boundary layer flow of a 2-D hybrid nanofluid. The research is designed to explore the rate of heat and mass transmission of carbon nanotubes-graphene in a Casson hybrid nanofluid over an exponentially stretching surface (ESS).

1.2 Definitions

1. A nanoparticle is a solid particle that has a diameter between 1 and 100 nanometres.
2. A base fluid is any fluid in which nanoparticles are suspended.
3. Nanofluid is a class of fluids obtained by suspending nanoparticles in a base fluid.

4. A hybrid nanofluid is a group of fluids formed when two different nanoparticles are suspended in one base fluid.

1.3 Statement of the Problem

Previous research on hybrid nanofluids concentrated majorly on the thermophysical and heat transfer enhancement properties. As a consensus, the superiority of the hybrid's properties over nanofluids and ordinary fluids are emphasized. Since carbon is the strongest, most abundant and a very good thermally conducting compound, the prospect of it being the best nanoparticle in enhancing the HAMT rate of the hybrid nanofluid is high. CNTs and graphene are allotropes of Carbon. So far, no researcher has explored the impact of suspending a combination of CNTs and graphene nanoparticles on a Casson base fluid in the HAMT rates study. To bridge this gap, this research is aimed at investigating HAMT rates of MHD hybrid Casson nanofluids. The carbon nanotubes (CNTs) and graphene are the choice nanoparticles for this study and the surface is exponentially stretching. The effects of volume fraction size, nanoparticle shapes and other pertinent parameters like radiation and magnetic parameters shall be investigated on the rate of HAMT.

1.4 Justification

Emphasis have always been dynamics properties of hybrid nanofluid like temperature and velocity, and on the heat transfer rate. Different nanoparticles have been suspended during the hybridization process and HAMT of various hybrid nanofluids have been documented to have significantly improved. So far, no researcher has studied CNTs-graphene nanoparticles impact on the HAMT rate of hybrid Casson nanofluid. This research work is focused on analysing the impact of the volume fraction, radiation, buoyancy, magnetic field, among other various

parameters associated with the flow on the HAMT of hybrid Casson nanofluid when CNTs and graphene are used as nanoparticles over an ESS. Nondimensionalisation is done to the flow model. Shooting technique and R-K method are the numerical methods used in solving the nondimensionalised model. Simulations are done using MATLAB bvp4c.

1.5 Objectives

1.5.1 General Objective

This research work aims to analyse the MHD HAMT rate of CNTs-graphene Casson hybrid nanofluid.

1.5.2 Specific Objectives

The specific objectives of this study are to;

i. Determine the system of PDEs model for studying the HAMT rate of a hybrid Casson nanofluid.

ii. Use suitable similarity variables from existing literature to reduce the parameters and remodel the system into its dimensionless form.

iii. Simulate the effects of pertinent parameters on the fluid velocity, temperature, and concentration.

iv. Investigate the HAMT rate in hybrid Casson nanofluid flow over an ESS.

1.6 Significance

Based on the innumerable potential applications of hybrid nanofluids, this study has practical applications in manufacturing industries. The results from this research work shall provide information to industries in the distillation of alcohol, industrial cooling towers, electric device coolants, and automotive coolants. From the results and conclusion of this study, the industries will acquire knowledge on what parameters to increase to achieve minimal drag, maximum HAMT rate and faster velocity when carrying out various industrial preparation and manufacturing processes.

1.7 Basic Assumptions

The assumptions made in this study are that;

1. The flow is steady, incompressible, and 2-D.
2. The surface on which the flow is occurring is exponentially stretching in the positive x-direction.
3. The no-slip condition is taken into consideration.
4. The magnetic field has a constant magnetic field strength.

Chapter 2

Literature Review

The world is gradually evolving from the computer age into the artificial intelligence age and with this, high-performance gadgets are required. This poses a challenge to scientists all over to work on ways to resolve the issues that will arise from this imminent change. The improvement in fluid technology that brought about changes from ordinary fluids to nanofluids and then to hybrid nanofluids over the past two decades is a clear indication of how scientists are constantly working and coming up with better solutions each time. Issues like coolants for those high-performance gadgets are rapidly being solved by the growth of fluid science.

Takhar *et al.* (2000) study on the characteristics of fluid mass transfer led to the discovery that transfer rate is highly dependant on the rate of the reactions. Nahirnyak *et al.* (2006) researched on blood flow when it is clotted and came up with the referenced thermophysical properties values for the fluid model of Casson. Wang and Mujumdar (2008) carried out a detailed review of some literature on the heat transfer qualities of nanofluids. They proposed that the suspension of nanoparticles in a base fluid can only be properly investigated when considered as a two-phase mixture rather than a single-phase mixture.

Of many important properties that can be studied in hybrid nanofluid flow, the rate of heat transmission is of prime importance. Research done by Elias *et al.* (2013) shows that cylindrically shaped nanoparticles have better thermal conductivity than other differently shaped nanoparticles such as spherically shaped and blade-shaped nanoparticles. Hayat and Nadeem (2017) have developed a mathematical model to study the heat transfer improvement of hybrid nanofluids comprising silver and

copper-oxide in water. Heat is generated in the flow and a chemical reaction is considered to take place during the flow. The flow is considered across a rotating surface and simultaneously experiencing stretching. The results indicated the improvement in the heat transmission of the hybrid nanofluid compared to nanofluids and ordinary fluids. Huminic and Huminic (2018) reviewed several literature and concluded that hybrid nanofluids are a major enhancement in nanotechnology and there are still a couple of issues associated with preparation and stability of the hybridization process . Subhani and Nadeem (2018) considered a hybrid nanofluid whose base fluid is micropolar. The study carried out a theoretical comparison between the heat transmission rate of the ordinary micropolar fluid, the micropolar nanofluid and the hybrid micropolar nanofluid. The results agreed with the results of Hayat and Nadeem (2017) and they inferred the best heat transmission rate is found in the hybrid micropolar fluid. Sheikholeslami *et al.* (2019) explored the effects of an unsteady magnetic force on heat transmission in hybrid nanofluids and their results agreed with the results of Hayat and Nadeem (2017) and Subhani and Nadeem (2018). They reiterated that heat transmission is drastically improved in hybrid nanofluid when compared with the ordinary base fluid or a nanofluid of similar individual nanoparticles. Babar and Ali (2019) further reviewed available literature and recommended ways of making the hybridization process cheaper. Bhattad and Sarkar (2019) emphasized the significant impact the nanoparticle shape and size on the rate of heat transfer. Jiang *et al.* (2019) and Ekiciler *et al.* (2020) further recapitulated the significance of nanoparticle shape on the enhancement of heat transfer as highlighted by Elias *et al.* (2013) and Bhattad and Sarkar (2019). Waini *et al.* (2019)explored the semi-analytical solutions of an unsteady flow of a hybrid nanofluid and their results showed two solutions are obtained; where one solution is stable while the other is not stable. Zainal *et al.* (2020) explained the results of Waini *et al.* (2019) by showing that only one of the solutions is significant for the research study. The other solution is only useful for mathematical completeness. Tassaddiq *et al.* (2020) took a more detailed look into the flow of a hybrid nanofluid with an

incompressible base fluid in a rotating disk. After a detailed analysis of different pairs of nanoparticles in the base fluid, they concluded that some nanoparticles like Carbon nanotubes greatly improve the heat transfer rate than many others. Bibi *et al.* (2020) documented that platelet shaped nanoparticles presented a higher heat enhancement rate. Hussain *et al.* (2020) documented various thermophysical properties values for Graphene. Othman *et al.* (2021) and Oke *et al.* (2021) elucidated the significance of magnetic field strength, gravitational force, and a heat source or sink on the flow of hybrid nanofluid over an ESS. Bilal *et al.* (2021) came up with the thermophysical properties values for the SWCNTs. Kigio *et al.* (2021) researched on volume fraction impact on nanofluid flow when the surface is uniform. Nandeppanavar *et al.* (2022) analysed in detail convective Casson nanofluid flow. The results indicated that drag, buoyancy and heat transfer increase as the Biot number surges. Juma *et al.* (2022) analysed the effects of both Coriolis and Lorentz forces on a magnetic fluid flow. They recorded a decrease in the drag when the inclined surface rotation is increased. Roy and Pop (2022) concluded that the dual solution's domain of existence increases as volume fraction and buoyancy surge. Using physics as an approach, Pathak *et al.* (2022) explains the reasons behind the surge in the output of thermal nanofluids. Oke *et al.* (2022) studied a 3-D ternary water hybrid nanofluid. The results indicates that the flow velocity increases in the y- direction as the stretch is increased.

The above-reviewed literature shows some of the unrelenting attempts by mathematicians and scientists to unravel the influence of suspending more than one nanoparticle in a base fluid. These efforts have shown that hybrid nanofluid provides the best improvement when compared with the novel fluid or nanofluid. But, none of the above literature considered the effects of volume fraction and different shapes of CNTs- graphene nanoparticles on the rate of HAMT of Casson base fluid. The present research shall focuses on the HAMT rate in MHD flow of a hybrid nanofluid formed from the suspension of CNTs and graphene in a Casson base fluid. The flow shall be considered across an ESS. The effects of volume fraction size, nanoparticle shapes and other pertinent parameters such as buoyancy shall be investigated on the HAMT rate.

Chapter 3

Methodology

3.1 Formulation of Governing Equations

The physical configuration of the flow is depicted in figure (3.1). A Casson base fluid is chosen for this study in which two nanoparticles; namely carbon nanotubes and graphenes- are suspended. The resulting hybrid nanofluid is allowed to flow across a surface in which a magnetic field is applied normal to the surface. The surface is stretching at an exponential rate so that the fluid layers adjacent to the wall have the same stretching velocity.

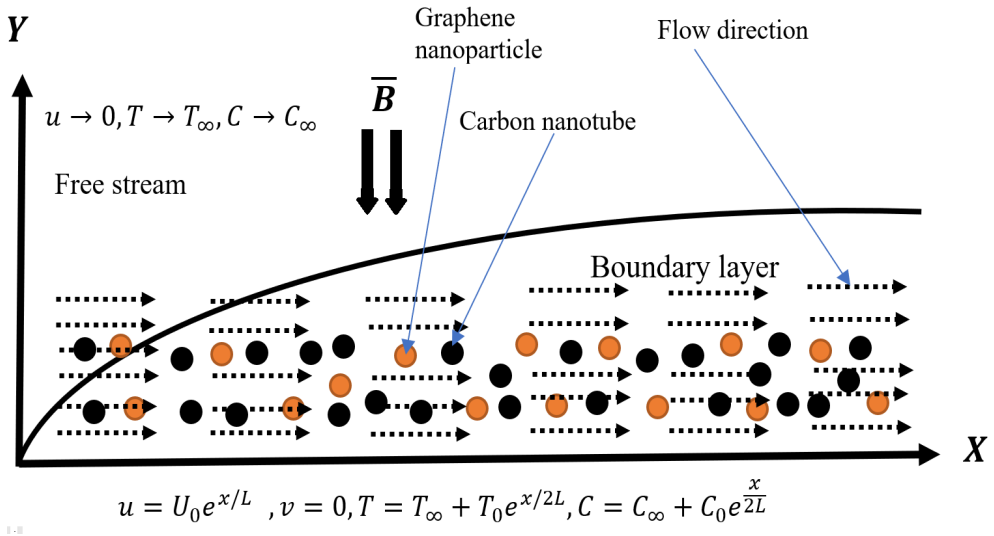

Figure 3.1: Flow prototype

Adopting the Buongiorno model to correct the dimensionless units, and after the boundary layer analysis, equations governing the flow under consideration are respectively

$$\frac{\partial u}{\partial x}+\frac{\partial v}{\partial y} = 0, \tag{3.1.1}$$

$$u\frac{\partial u}{\partial x}+v\frac{\partial u}{\partial y} = \left(1+\frac{1}{\gamma}\right)\frac{\mu_{hnf}}{\rho_{hnf}}\frac{\partial^2 u}{\partial y^2}+g\beta\left(T-T_\infty\right)-\frac{\sigma_{hnf}}{\rho_{hnf}}B_0^2 u, \tag{3.1.2}$$

$$u\frac{\partial T}{\partial x}+v\frac{\partial T}{\partial y} = \alpha_{hnf}\frac{\partial^2 T}{\partial y^2}+\frac{1}{(\rho C_p)_{hnf}}\frac{\partial q}{\partial y}+\tau\left(\frac{D_B}{\Delta C}\frac{\partial C}{\partial y}\frac{\partial T}{\partial y}+\frac{D_T}{T_\infty}\frac{\partial T}{\partial y}\frac{\partial T}{\partial y}\right), \tag{3.1.3}$$

$$u\frac{\partial C}{\partial x}+v\frac{\partial C}{\partial y} = D_B\frac{\partial^2 C}{\partial y^2}+\frac{D_T\Delta C}{T_\infty}\frac{\partial^2 T}{\partial y^2}. \tag{3.1.4}$$

subject to the no-slip boundary and initial conditions

$$\text{at } y=0: u=U_0 e^{x/L},\ v=0,\ T=T_\infty+T_0 e^{x/2L},\ C=C_\infty+C_0 e^{x/2L} \tag{3.1.5}$$

$$\text{as } y\to\infty: u\to 0,\ T\to T_\infty,\ C\to C_\infty. \tag{3.1.6}$$

where all variables are as defined in the nomenclature and

$$\frac{\partial q}{\partial y}=\frac{16\sigma^* T_\infty^3}{3K^*}\frac{\partial^2 T}{\partial y^2}.$$

The quantities of practical interest are the coefficient of skin friction, Nusselt number, and Sherwood number given as

$$C_f=\frac{\tau_w}{\rho_f U_w^2},\ N_u=\frac{x q_w}{K_{hnf}\left(T_w-T_\infty\right)},\ S_h=\frac{x J_w}{D_B\left(C_w-C_\infty\right)},$$

where

$$\tau_w=\mu_{hnf}\left(1+\frac{1}{\gamma}\right)\left.\frac{\partial u}{\partial y}\right|_{y=0},\ q_w=-K_{hnf}\left.\frac{\partial T}{\partial y}\right|_{y=0},\ J_w=-D_B\left.\frac{\partial C}{\partial y}\right|_{y=0}.$$

3.2 Similarity Transformation

Solving a PDEs is very strenuous and sometimes impossible. To curb this, the PDEs model is reduced to an ODEs system using similarity variables. This is done because, solving ODEs is simpler and many ODEs have unique solutions. The appropriate similarity variables for the system of equations (3.1.1 - 3.1.4) with the boundary conditions (3.1.5 - 3.1.6) is given as

$$\eta = y\left(\frac{U_0}{2\nu_f L}\right)^{1/2} e^{x/2L},\ u = U_0 e^{x/L} f',\ v = -\left(\frac{U_0\nu_f}{2L}\right)^{1/2} e^{x/2L}\left[\eta f' + f\right],$$
$$T = T_\infty + T_0 e^{x/2L}\Theta, \quad C = C_\infty + C_0 e^{x/2L}\Phi. \tag{3.2.1}$$

With these variables, all dimensions in the equations are removed and the independent variables are reduced from two to one. The variable η represents the dimensionless distance. f' and f are the dimensionless velocities in the x- and y-directions. The dimensionless temperature and concentration functions are Θ and Φ respectively. To start with, obtain the the partial derivatives of the dimensionless distance as follows;

$$\frac{\partial\eta}{\partial x} = \frac{y}{2L}\left(\frac{U_0}{2\nu_f L}\right)^{1/2} e^{x/2L}, \quad \frac{\partial\eta}{\partial y} = \left(\frac{U_0}{2\nu_f L}\right)^{1/2} e^{x/2L}.$$

From here, the derivatives of u are obtained as

$$\frac{\partial u}{\partial x} = U_0\frac{\partial}{\partial x}\left(e^{x/L}f'\right) = U_0\left(\frac{e^{x/L}}{L}f' + e^{x/L}\frac{df'}{d\eta}\frac{\partial\eta}{\partial x}\right) = \frac{U_0}{L}e^{x/L}\left(f' + \frac{y}{2}e^{x/2L}\left(\frac{U_0}{2\nu_f L}\right)^{1/2} f''\right),$$
$$\frac{\partial u}{\partial y} = \frac{\partial}{\partial y}\left(U_0 e^{x/L}f'\right) = U_0 e^{x/L}\frac{df'}{d\eta}\frac{\partial\eta}{\partial y} = U_0\left(\frac{U_0}{2\nu_f L}\right)^{1/2} e^{3x/2L} f'',$$
$$\frac{\partial^2 u}{\partial y^2} = \frac{\partial}{\partial y}\left(U_0\left(\frac{U_0}{2\nu_f L}\right)^{1/2} e^{3x/2L} f''\right) = U_0\left(\frac{U_0}{2\nu_f L}\right)^{1/2} e^{3x/2L}\frac{df''}{d\eta}\frac{\partial\eta}{\partial y} = \frac{U_0^2}{2\nu_f L}e^{2x/L} f'''$$

and the derivative of v with respect to y is obtained as

$$\frac{\partial v}{\partial y} = \frac{\partial}{\partial y}\left(-\left(\frac{U_0\nu_f}{2L}\right)^{1/2} e^{x/2L}\left[\eta f' + f\right]\right) = -\frac{U_0}{L}e^{x/L}f' - \frac{yU_0}{2L}\left(\frac{U_0}{2\nu_f L}\right)^{1/2} e^{3x/2L}f''.$$

The derivatives of the temperature are expressed in terms of the dimensionless temperature and are obtained as follows;

$$\begin{aligned}
\frac{\partial T}{\partial x} &= \frac{T_0}{2L}e^{x/2L}\Theta + T_0 e^{x/2L}\frac{d\Theta}{d\eta}\frac{\partial \eta}{\partial x} = \frac{T_0}{2L}e^{x/2L}\Theta + \frac{T_0 y}{2L}\left(\frac{U_0}{2\nu_f L}\right)^{1/2} e^{x/L}\Theta', \\
&= \frac{T_0}{2L}e^{x/2L}\left(\Theta + y\left(\frac{U_0}{2\nu_f L}\right)^{1/2} e^{x/2L}\Theta'\right). \\
\frac{\partial T}{\partial y} &= T_0 e^{x/2L}\frac{d\Theta}{d\eta}\frac{\partial \eta}{\partial y} = \left(\frac{U_0}{2\nu_f L}\right)^{1/2} T_0 e^{x/L}\Theta'. \\
\frac{\partial^2 T}{\partial y^2} &= \left(\frac{U_0}{2\nu_f L}\right)^{1/2} T_0 e^{x/L}\frac{d\Theta'}{d\eta}\frac{\partial \eta}{\partial y} = \frac{T_0 U_0}{2\nu_f L}e^{3x/2L}\Theta''.
\end{aligned}$$

The derivatives of the concentration are expressed in terms of the dimensionless concentration and are obtained as follows;

$$\begin{aligned}
\frac{\partial C}{\partial x} &= \frac{C_0}{2L}e^{x/2L}\Phi + C_0 e^{x/2L}\frac{d\Phi}{d\eta}\frac{\partial \eta}{\partial x} = \frac{C_0}{2L}e^{x/2L}\Phi + \frac{C_0 y}{2L}\left(\frac{U_0}{2\nu_f L}\right)^{1/2} e^{x/L}\Phi', \\
&= \frac{C_0}{2L}e^{x/2L}\left(\Phi + y\left(\frac{U_0}{2\nu_f L}\right)^{1/2} e^{x/2L}\Phi'\right). \\
\frac{\partial C}{\partial y} &= C_0 e^{x/2L}\frac{d\Phi}{d\eta}\frac{\partial \eta}{\partial y} = \left(\frac{U_0}{2\nu_f L}\right)^{1/2} C_0 e^{x/L}\Phi'. \\
\frac{\partial^2 C}{\partial y^2} &= \left(\frac{U_0}{2\nu_f L}\right)^{1/2} C_0 e^{x/L}\frac{d\Phi'}{d\eta}\frac{\partial \eta}{\partial y} = \frac{C_0 U_0}{2\nu_f L}e^{3x/2L}\Phi''.
\end{aligned}$$

The momentum equation (3.1.2);

$$u\frac{\partial u}{\partial x} + v\frac{\partial u}{\partial y} = \left(1 + \frac{1}{\gamma}\right)\frac{\mu_{hnf}}{\rho_{hnf}}\frac{\partial^2 u}{\partial y^2} + g^*\beta\left(T - T_\infty\right) - \frac{\sigma_{hnf}}{\rho_{hnf}}B_0^2 u,$$

is nondimensionalised as follows;

$$\begin{aligned}
LHS =& U_0 e^{x/L} f' \frac{U_0}{L} e^{x/L} \left(f' + \frac{y}{2} e^{x/2L} \left(\frac{U_0}{2\nu_f L} \right)^{1/2} f'' \right) \\
& - \left(\frac{U_0 \nu_f}{2L} \right)^{1/2} e^{x/2L} \left[\eta f' + f \right] U_0 \left(\frac{U_0}{2\nu_f L} \right)^{1/2} e^{3x/2L} f'' \\
=& \frac{U_0^2}{L} e^{2x/L} \left((f')^2 + \frac{y}{2} e^{x/2L} \left(\frac{U_0}{2\nu_f L} \right)^{1/2} f' f'' \right) - \frac{U_0^2}{2L} e^{2x/L} \left(\eta f' f'' + f f'' \right) \\
=& \frac{U_0^2}{L} e^{2x/L} (f')^2 + \frac{y U_0^2}{2L} e^{5x/2L} \left(\frac{U_0}{2\nu_f L} \right)^{1/2} f' f'' \\
& - \frac{y U_0^2}{2L} \left(\frac{U_0}{2\nu_f L} \right)^{1/2} e^{5x/2L} f' f'' - \frac{U_0^2}{2L} e^{2x/L} f f'' \\
=& \frac{U_0^2}{L} e^{2x/L} (f')^2 - \frac{U_0^2}{2L} e^{2x/L} f f'' = \frac{U_0^2}{2L} e^{2x/L} \left(2 (f')^2 - f f'' \right)
\end{aligned} \tag{3.2.2}$$

$$\begin{aligned}
RHS =& \left(1 + \frac{1}{\gamma} \right) \frac{U_0^2}{2\nu_f L} \frac{\mu_{hnf}}{\rho_{hnf}} e^{2x/L} f''' + g\beta \left(T_0 e^{x/2L} \Theta \right) - \frac{\sigma_{hnf}}{\rho_{hnf}} B_0 U_0 e^{x/L} f' \\
=& \left(1 + \frac{1}{\gamma} \right) \frac{U_0^2}{2\nu_f L} \frac{\mu_{hnf}}{\rho_{hnf}} e^{2x/L} f''' + g\beta \left(T_0 e^{x/2L} \Theta \right) - \frac{\sigma_{hnf}}{\rho_{hnf}} B_0 U_0 e^{x/L} f' \qquad (3.2.3) \\
=& \frac{U_0^2}{2L} e^{2x/L} \left\{ \left(1 + \frac{1}{\gamma} \right) \frac{\mu_{hnf}}{\rho_{hnf}} \frac{1}{\nu_f} f''' + \frac{2L g \beta T_0}{U_0^2} e^{-3x/2L} \Theta - \frac{2L \sigma_{hnf} B_0}{\rho_{hnf} U_0} e^{-x/L} f' \right\} \\
=& \frac{U_0^2}{2L} e^{2x/L} \left\{ \left(1 + \frac{1}{\gamma} \right) \frac{\mu_{hnf}}{\rho_{hnf}} \frac{1}{\nu_f} f''' + 2Gr\Theta - 2Mf' \right\} \qquad (3.2.4)
\end{aligned}$$

where;

$$Gr = \frac{L g \beta T_0 e^{-3x/2L}}{U_0^2}, \quad M = \frac{L \sigma_{hnf} B_0}{U_0 \rho_{hnf}} e^{-x/L}.$$

Therefore, equation (3.2.2) and (3.2.4) and rearranging gives;

$$\left(1 + \frac{1}{\gamma} \right) \frac{\mu_{hnf}}{\rho_{hnf}} \frac{1}{\nu_f} f''' + 2Gr\Theta - 2Mf' - 2 (f')^2 + f f'' = 0.$$

From the effective dynamic viscosity and density of the hybrid nanofluid given as

$$\mu_{hnf} = \frac{\mu_f}{(1-\phi)^{5/2}}, \text{ where } \phi = \phi_1 + \phi_2$$
$$\rho_{hnf} = (1-\phi)\rho_f + \phi_1\rho_1 + \phi_2\rho_2 = \left(1 - \phi + \phi_1\frac{\rho_1}{\rho_f} + \phi_2\frac{\rho_2}{\rho_f}\right)\rho_f$$

and hence

$$\frac{\mu_{hnf}}{\rho_{hnf}}\frac{1}{\nu_f} = \frac{(1-\phi)^{-5/2}\mu_f}{\left(1-\phi+\phi_1\frac{\rho_1}{\rho_f}+\phi_2\frac{\rho_2}{\rho_f}\right)\rho_f\nu_f} = \frac{(1-\phi)^{-5/2}}{1-\phi+\phi_1\frac{\rho_1}{\rho_f}+\phi_2\frac{\rho_2}{\rho_f}} = A_1,$$

and therefore, the dimensionless form of the momentum equation is

$$\left(1+\frac{1}{\gamma}\right)A_1 f''' + 2Gr\Theta - 2Mf' - 2\left(f'\right)^2 + ff'' = 0. \tag{3.2.5}$$

The energy equation (3.1.3);

$$u\frac{\partial T}{\partial x} + v\frac{\partial T}{\partial y} = \alpha_{hnf}\frac{\partial^2 T}{\partial y^2} + \frac{1}{(\rho C_p)_{hnf}}\frac{\partial q}{\partial y} + \tau\left(\frac{D_B}{\Delta C}\frac{\partial C}{\partial y}\frac{\partial T}{\partial y} + \frac{D_T}{T_\infty}\frac{\partial T}{\partial y}\frac{\partial T}{\partial y}\right),$$

is nondimensionalised as follows;

$$\begin{aligned}
LHS =& U_0 e^{x/L} f'\left\{\frac{T_0}{2L}e^{x/2L}\left(\Theta + y\left(\frac{U_0}{2\nu_f L}\right)^{1/2} e^{x/2L}\Theta'\right)\right\} \\
&- \left(\frac{U_0\nu_f}{2L}\right)^{1/2} e^{x/2L}\left[\eta f' + f\right]\left(\frac{U_0}{2\nu_f L}\right)^{1/2} T_0 e^{x/L}\Theta' \\
=& \frac{U_0 T_0}{2L}e^{3x/2L}\Theta f' + \frac{U_0 T_0 y}{2L}\left(\frac{U_0}{2\nu_f L}\right)^{1/2} e^{2x/L}\Theta' f' \\
&- \frac{U_0 T_0}{2L}e^{3x/2L}\Theta' f - \frac{U_0 T_0 y}{2L}\left(\frac{U_0}{2\nu_f L}\right)^{1/2} e^{2x/L} f'\Theta' \\
=& \frac{U_0 T_0}{2L}e^{3x/2L}\left\{\Theta f' - \Theta' f\right\}.
\end{aligned} \tag{3.2.6}$$

$$
\begin{aligned}
RHS =& \alpha_{hnf}\frac{T_0U_0}{2\nu_f L}e^{3x/2L}\Theta'' + \frac{16\sigma^*T_\infty^3T_0U_0}{3K^*\left(\rho C_\rho\right)_{hnf}2\nu_f L}e^{3x/2L}\Theta'' \\
&+ \tau\left[\frac{D_B}{\Delta C}\frac{C_0U_0T_0}{2\nu_f L}e^{2x/L}\Theta'\Phi' + \frac{D_T}{T_\infty}\frac{T_0^2U_0}{2\nu_f L}e^{2x/L}\left(\Theta'\right)^2\right], \\
&= \frac{U_0T_0}{2L}e^{3x/2L}\left[\left(\frac{\alpha_{hnf}}{\nu_f} - \frac{16\sigma^*T_\infty^3}{3K^*\left(\rho C_\rho\right)_{hnf}\nu_f}\right)\Theta'' + \tau e^{x/2L}\left[\frac{D_B}{\Delta C}\frac{C_0}{\nu_f}\Theta'\Phi' + \frac{D_T}{T_\infty}\frac{T_0}{\nu_f}\left(\Theta'\right)^2\right]\right]
\end{aligned}
\tag{3.2.7}
$$

By equating (3.2.6) to (3.2.7) and rearranging gives

$$
\left(\frac{\alpha_{hnf}}{\nu_f} + \frac{16\sigma^*T_\infty^3}{3K^*\left(\rho C_\rho\right)_{hnf}\nu_f}\right)\Theta'' + \tau e^{x/2L}\left[\frac{D_B}{\Delta C}\frac{C_0}{\nu_f}\Theta'\Phi' + \frac{D_T}{T_\infty}\frac{T_0}{\nu_f}\left(\Theta'\right)^2\right] - \Theta f' + \Theta' f = 0
$$

but, the thermal conductivity is given by the formula $\alpha_{hnf} = \frac{K_{hnf}}{\left(\rho C_\rho\right)_{hnf}}$ where

$$
\begin{aligned}
\frac{K_{hnf}}{K_f} &= \left\{\frac{\left(1+2\phi\right)\left(\phi_1K_1+\phi_2K_2\right)+2\left(1-\phi\right)\phi K_f}{\left(1-\phi\right)\left(\phi_1K_1+\phi_2K_2\right)+\left(2+\phi\right)\phi K_f}\right\} = A \\
\frac{\left(\rho C_\rho\right)_{hnf}}{\left(\rho C_\rho\right)_f} &= \left\{\left(1-\phi\right)+\frac{\phi_1\left(\rho C_\rho\right)_1}{\left(\rho C_\rho\right)_f}+\frac{\phi_2\left(\rho C_\rho\right)_2}{\left(\rho C_\rho\right)_f}\right\} = B \\
\Rightarrow \alpha_f &= \frac{K_f}{\left(\rho C_\rho\right)_f},\ A_2 = \frac{A}{B} \quad \text{and} \quad \alpha_{_{hnf}} = \frac{AK_f}{B\left(\rho C_\rho\right)_f} = A_2\alpha_f
\end{aligned}
$$

and also

$$
\begin{aligned}
\frac{16\sigma^*T_\infty^3}{3K^*\left(\rho C_\rho\right)_{hnf}\nu_f} &= \frac{4}{3}\frac{4\sigma^*T_\infty^3}{K^*\left(\rho C_\rho\right)_{hnf}}\frac{1}{\nu_f} = \frac{4}{3}\frac{4\sigma^*T_\infty^3}{K^*\left(\frac{K_{hnf}}{\alpha_{hnf}}\right)}\frac{1}{\nu_f} \\
&= \frac{4}{3}\frac{4\sigma^*T_\infty^3}{K^*K_{hnf}}\frac{\alpha_{hnf}}{\nu_f} = \frac{4}{3}\frac{4\sigma^*T_\infty^3}{\alpha_{hnf}K^*}\frac{A_2\alpha_f}{\nu_f} = \frac{4}{3}R\frac{A_2\alpha_f}{\nu_f}
\end{aligned}
$$

where

$$
R = \frac{4\sigma^*T_\infty^3}{K^*K_{hnf}}
$$

therefore,

$$\left(\frac{A_2\alpha_f}{\nu_f}+\frac{4}{3}R\frac{A_2\alpha_f}{\nu_f}\right)\Theta''+\tau e^{x/2L}\left[\frac{D_B}{\Delta C}\frac{C_0}{\nu_f}\Theta'\Phi'+\frac{D_T}{T_\infty}\frac{T_0}{\nu_f}\left(\Theta'\right)^2\right]-\Theta f'+\Theta' f=0$$

$$A_2\frac{\alpha_f}{\nu_f}\left(1+\frac{4}{3}R\right)\Theta''+\tau e^{x/2L}\left[\frac{D_B}{\Delta C}\frac{C_0}{\nu_f}\Theta'\Phi'+\frac{D_T}{T_\infty}\frac{T_0}{\nu_f}\left(\Theta'\right)^2\right]-\Theta f'+\Theta' f=0$$

$$A_2\left(1+\frac{4}{3}R\right)\Theta''+\tau e^{x/2L}\left[\frac{D_B}{\Delta C}\frac{C_0}{\alpha_f}\Theta'\Phi'+\frac{D_T}{T_\infty}\frac{T_0}{\alpha_f}\left(\Theta'\right)^2\right]-\frac{\nu_f}{\alpha_f}\Theta f'+\frac{\nu_f}{\alpha_f}\Theta' f=0$$

Setting

$$Pr=\frac{\nu_f}{\alpha_f},\ N_t=\frac{D_T}{T_\infty}\frac{T_0}{\alpha_f}\tau e^{x/2L},\ N_b=\frac{D_B}{\Delta C}\frac{C_0}{\alpha_f}\tau e^{x/2L},$$

then the energy equation becomes;

$$A_1\left(1+\frac{4}{3}R\right)\Theta''+N_b\Theta'\Phi'+N_t\left(\Theta'\right)^2-Pr\Theta f'+Pr\Theta' f=0. \tag{3.2.8}$$

Finally, the concentration equation

$$u\frac{\partial C}{\partial x}+v\frac{\partial C}{\partial y}=D_B\frac{\partial^2 C}{\partial y^2}+\frac{D_T\Delta C}{T_\infty}\frac{\partial^2 T}{\partial y^2},$$

is rendered dimensionless as follows;

$$\begin{aligned}LHS=&U_0e^{x/L}f'\frac{C_0}{2L}e^{x/2L}\left(\Phi+y\left(\frac{U_0}{2\nu_fL}\right)^{1/2}e^{x/2L}\Phi'\right)\\&-\left(\frac{U_0\nu_f}{2L}\right)^{1/2}e^{x/2L}\left[\eta f'+f\right]\left(\frac{U_0}{2\nu_fL}\right)^{1/2}C_0e^{x/L}\Phi'\\=&\frac{U_0C_0}{2L}e^{3x/2L}f'\Phi+\frac{yU_0C_0}{2L}\left(\frac{U_0}{2\nu_fL}\right)^{1/2}e^{2x/L}f'\Phi'\\&-\frac{yU_0C_0}{2L}\left(\frac{U_0}{2\nu_fL}\right)^{1/2}e^{2x/L}f'\Phi'-\frac{U_0C_0}{2L}e^{3x/2L}f\Phi'\\=&\frac{U_0C_0}{2L}e^{3x/2L}\left\{f'\Phi-f\Phi'\right\}.\end{aligned}$$

$$RHS = D_B \frac{U_0 C_0}{2\nu_f L} e^{3x/2L}\Phi'' + D_\tau \frac{\Delta C T_0 U_0}{T_\infty 2\nu_f L} e^{3x/2L}\Theta''.$$
$$= \frac{U_0 C_0}{2L} e^{3x/2L}\left\{ \frac{D_B}{\nu_f}\Phi'' + \frac{D_B}{\nu_f}\frac{N_t}{N_b}\Theta'' \right\}$$

Equating the left hand side and right hand side gives;

$$\frac{D_B}{\nu_f}\Phi'' + \frac{D_B}{\nu_f}\frac{N_t}{N_b}\Theta'' - f'\Phi + f\Phi' = 0, \text{ where } Sc = \frac{\nu_f}{D_B}.$$

Equation (3.1.4) becomes;

$$\Phi'' + \frac{N_t}{N_b}\Theta'' + Scf\Phi' - Scf'\Phi = 0. \tag{3.2.9}$$

The conditions $y = 0$ and $y \to \infty$ transform to $\eta = 0$ and $\eta \to \infty$ respectively and

$$\text{for } \eta = 0; u = U_0 e^{x/L} \Rightarrow U_0 e^{x/L} f' = U_0 e^{x/L} \Rightarrow f' = 1;$$
$$v = 0 \Rightarrow -\left(\frac{U_0 \nu_f}{2L}\right)^{1/2} e^{x/2L}\left(\eta f' + f\right) = 0 \Rightarrow f = 0;$$
$$T = T_\infty + T_0 e^{x/2L} \Rightarrow T_\infty + T_0 e^{x/2L}\Theta = T_\infty + T_0 e^{x/2L} \Rightarrow \Theta = 1;$$
$$C = C_\infty + C_0 e^{x/2L} \Rightarrow C_\infty + C_0 e^{x/2L}\Phi = C_\infty + C_0 e^{x/2L} \Rightarrow \Phi = 1$$
$$\text{as } \eta \to \infty; u \to 0 \Rightarrow U_0 e^{x/L} f' \to 0 \Rightarrow f' \to 0;$$
$$T \to T_\infty \Rightarrow T_\infty + T_0 e^{x/2L}\Theta \to T_\infty \Rightarrow \Theta \to 0;$$
$$C \to C_\infty \Rightarrow C_\infty + C_0 e^{x/2L}\Phi \to C_\infty \Rightarrow \Phi \to 0;$$

The dimensionless equations are

$$\left(1 + \frac{1}{\gamma}\right) A_1 f''' + 2Gr\Theta - 2Mf' - 2\left(f'\right)^2 + ff'' = 0,$$
$$A_2\left(1 + \frac{4}{3}R\right)\Theta'' + N_b\Theta'\Phi' + N_t\left(\Theta'\right)^2 - Pr\Theta f' + Pr\Theta' f = 0,$$
$$\Phi'' + \frac{N_t}{N_b}\Theta'' + Scf\Phi' - Scf'\Phi = 0. \tag{3.2.10}$$

with the boundary conditions

$$\begin{aligned} &\text{for } \eta = 0;\ f' = 1;\ f = 0;\ \Theta = 1;\ \Phi = 1 \\ &\text{as } \eta \to \infty;\ f' \to 0;\ \Theta \to 0;\ \Phi \to 0; \end{aligned} \tag{3.2.11}$$

where

$$A_1 = \frac{(1-\phi)^{-5/2}}{1-\phi+\phi_1\frac{\rho_1}{\rho_f}+\phi_2\frac{\rho_2}{\rho_f}},\ A_2 = \frac{\left\{\frac{(1+2\phi)(\phi_1K_1+\phi_2K_2)+2(1-\phi)\phi K_f}{(1-\phi)(\phi_1K_1+\phi_2K_2)+(2+\phi)\phi K_f}\right\}}{\left\{(1-\phi)+\frac{\phi_1\left(\rho C_\rho\right)_1}{\left(\rho C_\rho\right)_f}+\frac{\phi_2\left(\rho C_\rho\right)_2}{\left(\rho C_\rho\right)_f}\right\}}$$

$$Gr = \frac{Lg\beta T_0 e^{-3x/2L}}{U_0^2},\ M = \frac{L\sigma_{hnf}B_0}{U_0\rho_{hnf}}e^{-x/L},\ Sc = \frac{\nu_f}{D_B}\ Pr = \frac{\nu_f}{\alpha_f},$$

$$R = \frac{4\sigma^* T_\infty^3}{K^* K_{hnf}},\ N_t = \frac{D_T}{T_\infty}\frac{T_0}{\alpha_f}\tau e^{x/2L},\ N_b = \frac{D_B}{\Delta C}\frac{C_0}{\alpha_f}\tau e^{x/2L},$$

By setting

$$u_1 = f,\ u_2 = f',\ u_3 = f'',\ u_4 = \Theta,\ u_5 = \Theta',\ u_6 = \Phi,\ u_7 = \Phi'$$

the system of equation can be re-written as

$$u_1' = u_2, \tag{3.2.12}$$

$$u_2' = u_3, \tag{3.2.13}$$

$$u_3' = -\left(\left(1+\frac{1}{\gamma}\right)A_1\right)^{-1}\left(2Gru_4 - 2Mu_2 - 2u_2^2 + u_1u_3\right), \tag{3.2.14}$$

$$u_4' = u_5, \tag{3.2.15}$$

$$u_5' = -\left(A_2\left(1+\frac{4}{3}R\right)\right)^{-1}\left(N_bu_5u_7 + N_tu_5^2 - Pru_4u_2 + Pru_5u_1\right), \tag{3.2.16}$$

$$u_6' = u_7 \tag{3.2.17}$$

$$u_7' = -\left(\frac{N_t}{N_b}u_5' + Scu_1u_7 - Scu_2u_6\right) \tag{3.2.18}$$

with conditions given as

$$u_2(0) = 1;\ u_1(0) = 0;\ u_4(0) = 1;\ u_6(0) = 1 \tag{3.2.19}$$

$$u_2(\infty) \to 0;\ u_4(\infty) \to 0;\ u_6(\infty) \to 0. \tag{3.2.20}$$

3.3 Quantities of Interest

The dimensionless form of the skin friction is obtained as follows;

$$\begin{aligned}
C_f &= \frac{\tau_w}{\rho_f U_w^2} = \frac{\mu_f}{\rho_f U_w^2}\left(1+\frac{1}{\gamma}\right)\left.\frac{\partial u}{\partial y}\right|_{y=0},\\
C_f &= \frac{\mu_f}{\rho_f\left(U_0 e^{x/L}\right)^2}\left(1+\frac{1}{\gamma}\right)U_0\left(\frac{U_0}{2\nu_f L}\right)^{1/2} e^{3x/2L} f''(0),\\
C_f &= \frac{\mu_f}{\rho_f U_0}\left(1+\frac{1}{\gamma}\right)\left(\frac{U_0}{2\nu_f L}\right)^{1/2} e^{-x/2L} f''(0),\\
C_f &= \frac{\nu_f}{U_0}\left(\frac{U_0}{2\nu_f L}\right)^{1/2} e^{-x/2L}\left(1+\frac{1}{\gamma}\right) f''(0),\\
&\left(\frac{\nu_f}{2U_0 L}\right)^{-1/2} e^{x/2L} C_f = \left(1+\frac{1}{\gamma}\right) f''(0),\\
&Re^{1/2} C_f = \left(1+\frac{1}{\gamma}\right) f''(0).
\end{aligned}$$

The dimensionless form of the heat transfer rate is given by;

$$\begin{aligned}
N_u &= \frac{x q_w}{K_{hnf}(T_w - T_\infty)} = \frac{-x\left.\frac{\partial T}{\partial y}\right|_{y=0}}{T_w - T_\infty} = \frac{-x\left(\frac{U_0}{2\nu_f L}\right)^{1/2} T_0 e^{x/L}\Theta'(0)}{T_0 e^{x/2L}}\\
N_u &= -x\left(\frac{U_0}{2\nu_f L}\right)^{1/2} e^{x/2L}\Theta'(0) = -Re^{1/2}\Theta'(0)\\
&Re^{-1/2} N_u = -\Theta'(0)
\end{aligned}$$

The dimensionless form of the mass transfer rate is given by;

$$S_h = \frac{xJ_w}{D_B\left(C_w - C_\infty\right)} = \frac{-x\left.\frac{\partial C}{\partial y}\right|_{y=0}}{C_w - C_\infty} = \frac{-x\left(\frac{U_0}{2\nu_f L}\right)^{1/2} C_0 e^{x/L}\Phi'(0)}{C_0 e^{x/2L}}$$

$$S_h = -x\left(\frac{U_0}{2\nu_f L}\right)^{1/2} e^{x/2L}\Phi'(0) = -Re^{1/2}\Phi'(0)$$

$$Re^{-1/2}S_h = -\Phi'(0)$$

Hence, the quantities of interests are

$$C_f Re^{1/2} = \left(1 + \frac{1}{\gamma}\right) f''(0)\,,\ N_u Re^{-1/2} = -\Theta'(0)\,,\ Re^{-1/2}S_h = -\Phi'(0)\,.$$

3.4 Numerical Technique

3.4.1 Shooting Technique

Shooting Technique is a method used to convert boundary conditions to initial conditions. For IVPs, we can start from the initial value and solve using numerical methods. However, numerical methods do not work for BVPs since there are not insufficient initial value constraints to tackle the ODE and get a solution that is unique. Therefore, a shooting method was developed to overcome this difficulty. The name of the shooting method comes from the target shooting analogy: you can shoot a target, observe where it hits, and based on your error, adjust your aim and shoot again. In this research, the shooting technique is employed to transform the dimensionless BVP above [equation (3.2.12) to equation (3.2.20)] to its equivalent initial value problem. The conditions (3.2.19) and (3.2.20) are written as

$$u_1(0) = 0;\ u_2(0) = 1;\ u_3(0) = s_1;\ u_4(0) = 1; \tag{3.4.1}$$

$$u_5(0) = s_2;\ u_6(0) = 1;\ u_7(0) = s_3; \tag{3.4.2}$$

and solve the system of equations (3.2.12 - 3.2.18) with the same initial guesses for s_1, s_2, s_3 and the results are compared with the three free stream conditions (3.2.20). The guesses are updated based on error found in the comparison. The process is repeated until a tolerable error is achieved.

3.4.2 Runge Kutta (R-K) method

R-K method is an efficient and effective technique in solving IVPs. The use of this method enables one to increase the step size while still getting accurate solutions. R-K technique maintains the stability of a system as long as the step size chosen is not too large. The resulting IVP after the shooting technique is applied, is solved using the R-K fourth order method. The general R-K scheme used in solving the system of ODEs is given by;

$$\begin{cases} U_{n+1} = U_n + \frac{1}{6}(k_1 + 2k_2 + 2k_3 + k_4) \\ k_1 = hf(x_n, u_n) \\ k_2 = hf(x_n + \frac{h}{2}, u_n + \frac{k_1}{2}) \\ k_3 = hf(x_n + \frac{h}{2}, u_n + \frac{k_2}{2}) \\ k_4 = hf(x_n + h, u_n + k_3) \end{cases} \tag{3.4.3}$$

where h =step size

Chapter 4

Analysis of Results and Discussion

The system of (3.2.12 - 3.2.18) with the BCs (3.2.19 - 3.2.20) is simulated with default values of the parameters chosen as

$$Gr = 1;\ M = 1;\ \gamma = 10;\ N_b = N_t = 1;\ Pr = 7;\ R = 2;\ Sc = 0.63;\ \phi_1 = \phi_2 = 0.15$$

and the results are depicted as graphs which shall be presented for discussion. The thermophysical properties of the nanoparticles and the base fluid are shown in table (4.1). The effects of variation of different parameters on the concentration profile, temperature profile, and primary velocity are shown as graphs. An analysis of the resulting graphs and the possible reasons for the behaviour observed in the graphs are provided.

	ρ	c_p	K_1	Source
SWCNT	2600	425	6600	Bilal *et al.* (2021)
Graphene	2250	2100	2500	Hussain *et al.* (2020)
Blood	1093	3210	0.451	Nahirnyak *et al.* (2006)

Table 4.1: Thermophysical properties

4.1 Primary velocity

The effects of the parameters on the primary velocity are shown in Figures (4.1 - 4.6). Figure (4.1) displays that increasing the Casson parameter causes a decrease in the primary velocity. This is due to the increase in the viscous effects in the fluid when the Casson parameter is increased. The dynamic viscosity generates an opposing force to the fluid movement which results in decreases in the primary velocity. Grashof

number is a measure of buoyancy in the flow. Raising the buoyancy results in a reduction in the dynamic viscosity at the boundary layer, which in turn enhances fluid flow. Hence, increasing the Grashof number brings about an increase in the velocity profile as illustrated in figure (4.2). Figure (4.3) displays that primary velocity decreases with increasing Magnetic parameter. This can be traced to the fact that the presence of magnetic field generates Lorentz force which opposes fluid flow. Hence, increasing magnetic field strength leads to an increased Lorentz force which in turn, opposes fluid flow and thereby reduces velocity profiles. Figure (4.4) displays that the primary velocity increases with a simultaneous increase in the Brownian motion and thermophoretic parameter. The continuous collision of the suspended nanoparticles with each other and the wall of the stretching surface leads to increased kinetic energy in the flow. Figure (4.5) shows that primary velocity decreases with the Prandtl number. This is attributed to the increase in the momentum diffusivity which slows down the fluid flow thereby decreasing the velocity profile. The effect of radiation parameter on the primary velocity profiles is depicted in Figure (4.6). It is shown that there is a notable increase in the primary velocity when the Radiation parameter is increased. Increasing the Radiation parameter increases heat energy in the flow. The influx of heat excites the fluid particles which increase the flow velocity.

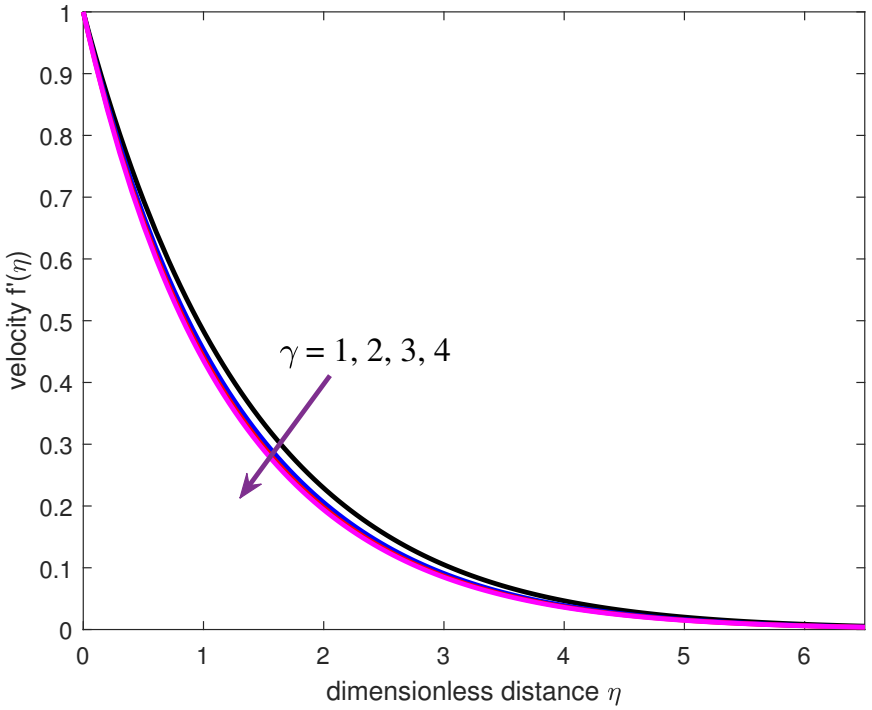

Figure 4.1: Primary velocity with Casson parameter

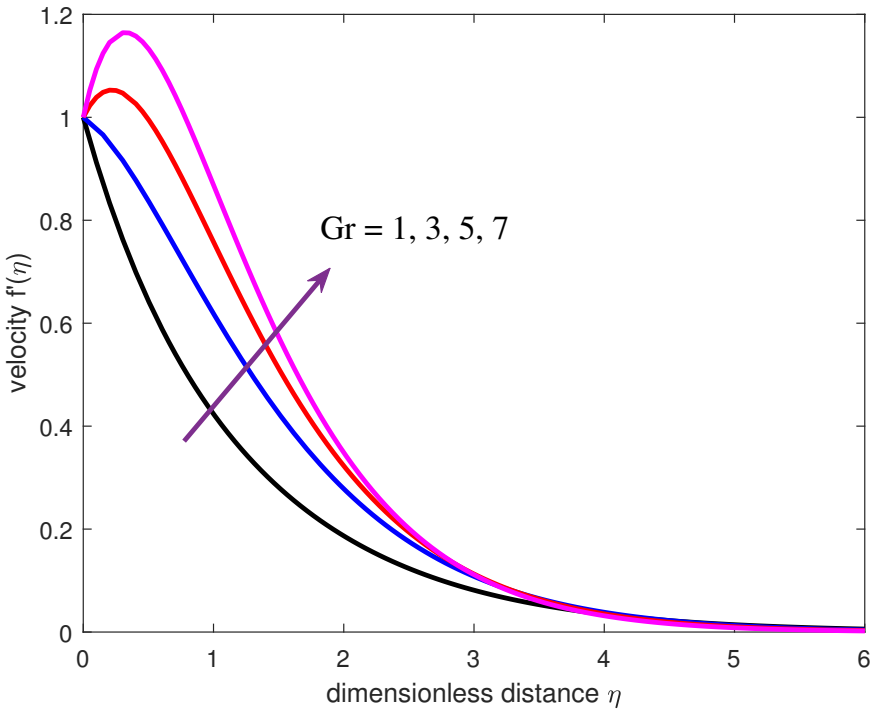

Figure 4.2: Primary velocity with Grashof number

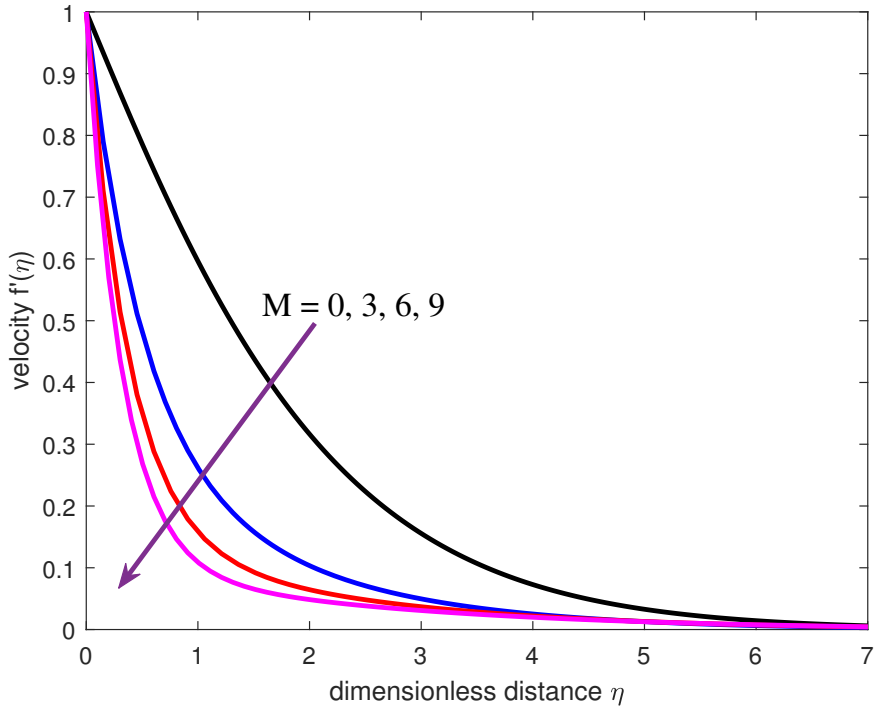

Figure 4.3: Primary velocity with Magnetic parameter

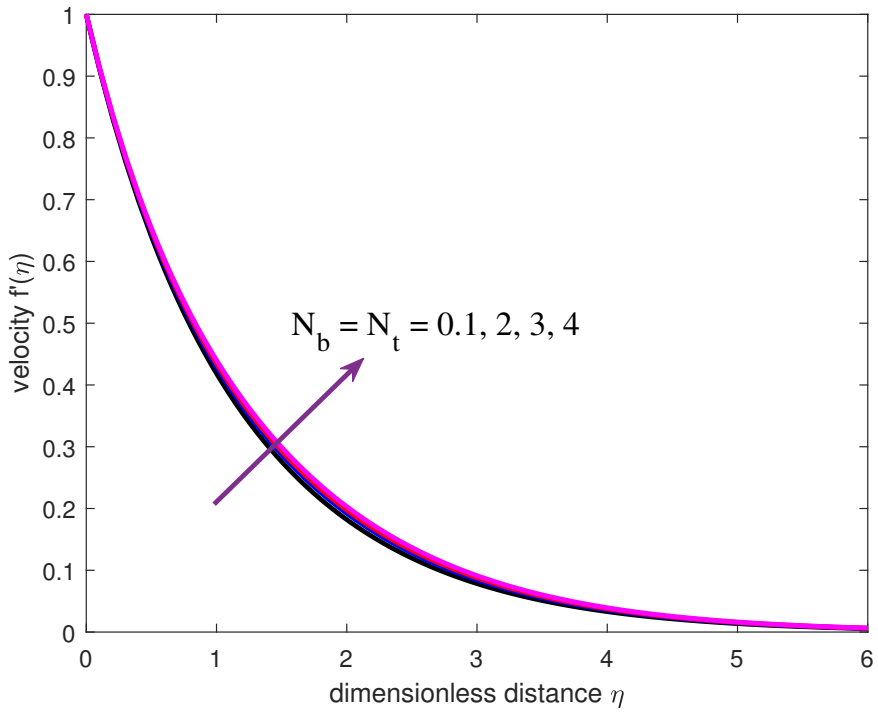

Figure 4.4: Primary velocity with Brownian motion parameter and Thermophoretic parameter

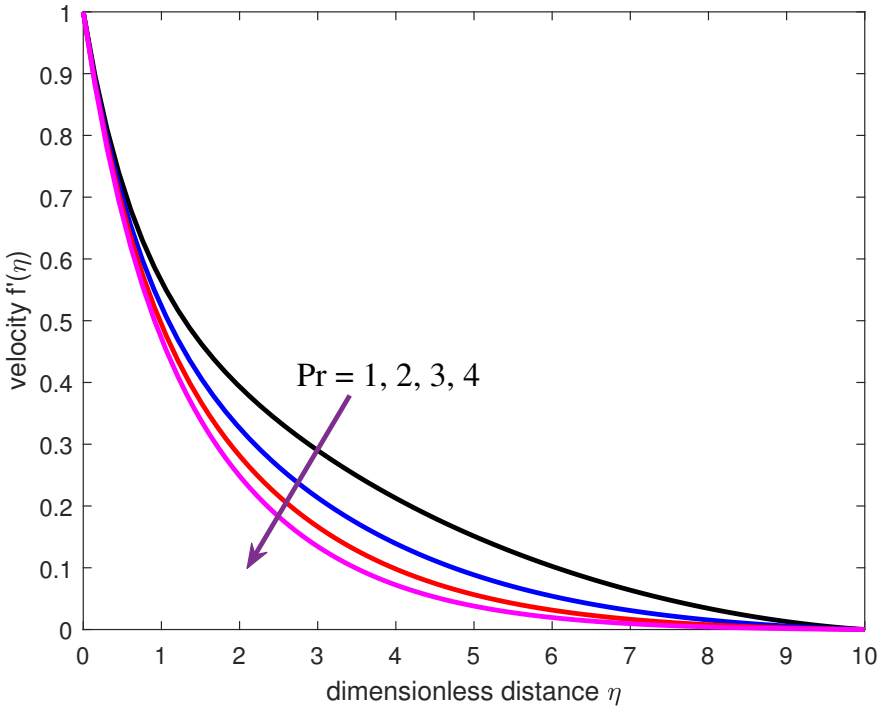

Figure 4.5: Primary velocity with Prandtl number

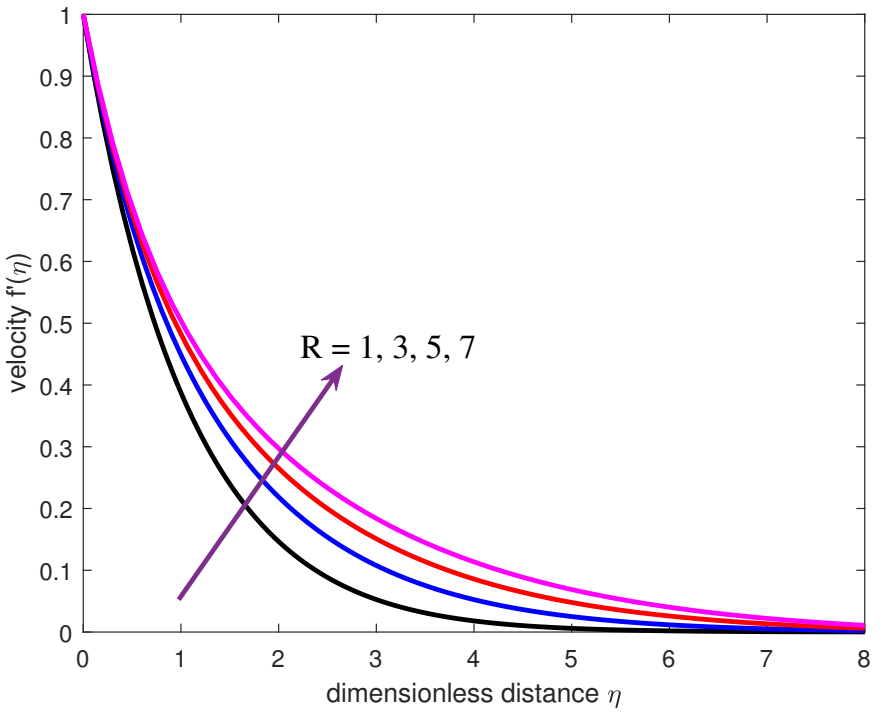

Figure 4.6: Primary velocity with Radiation parameter

4.2 Temperature profile

By varying the flow parameters, the temperature profiles are analysed and discussed in this section. Figure (4.7) displays that increasing the Casson parameter increases the temperature profile. When the Casson parameter is increased, heat is generated in the flow and the fluid layers heat up. This creates a surge in the temperature gradient and as a result, the thermal boundary layer increases. In figure (4.8), the temperature profile decreases as the Grashof number increases. When the Grashof number increases, heat energy is added to the molecules of the fluid. The fluid molecule gathers momentum and the extra heat energy is lost to the fluid environs. This loss reduces the drag generated in the flow leading to a decrease in the temperature profile. Figure (4.9) displays that increasing the Magnetic parameter increases the temperature profile. This is because Magnetic field generates Lorentz force which, in turn, generates internal energy. The additional internal energy is added in form of heat and that causes the temperature profile to increase with increasing magnetic field parameter. In figure (4.10), increasing the Brownian motion and Thermophoretic parameters causes a rise in the temperature profile. The simultaneous increase in the Brownian motion and the Thermophoretic parameters boosts nanoparticle motion which generates heat in the flow and thereby leads to an increase in the temperature profiles. Figure (4.11) displays that increasing the volume fraction increases the temperature profile. An increase in the volume fraction creates a surge in the thermal conductivity of the flow thereby leading to an increase in the temperature profile. In figure (4.12), the temperature profile decreases with an increase in the Prandtl number. As the Prandtl number increases, the thermal diffusivity decreases which result in thermal boundary layer thinning. As a result, this leads to a decrease in the temperature profile. Figure (4.13) depicts that increasing the Radiation parameter increases the temperature profile. This is due to the heat energy released into the flow when the Radiation parameter is increased. The fluid layers are heated and the temperature gradient is increased. This leads to an increase in the thermal boundary

layer and hence, a surge in the temperature profile.

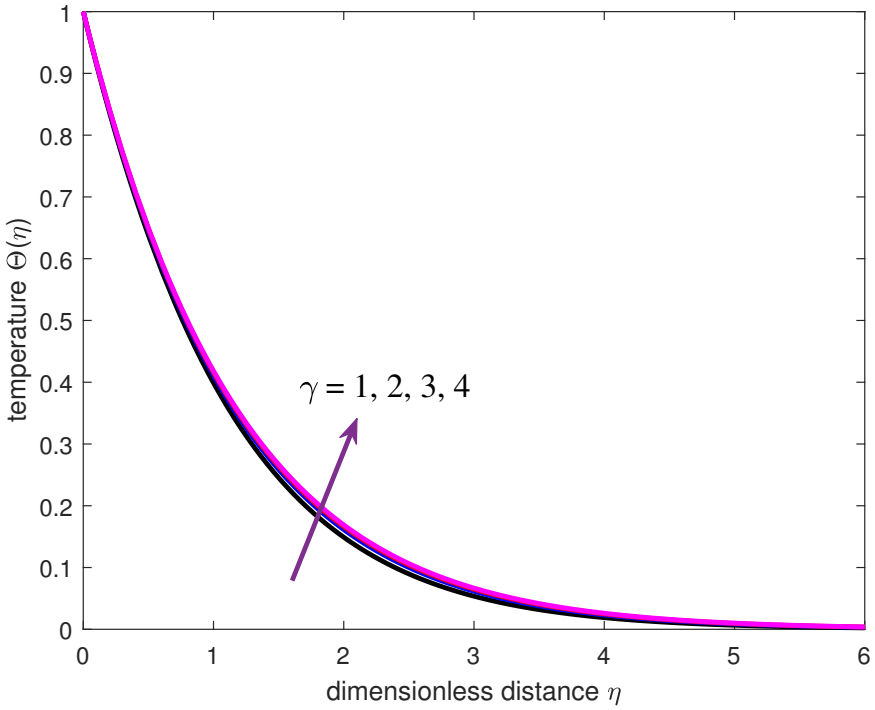

Figure 4.7: Temperature with Casson parameter

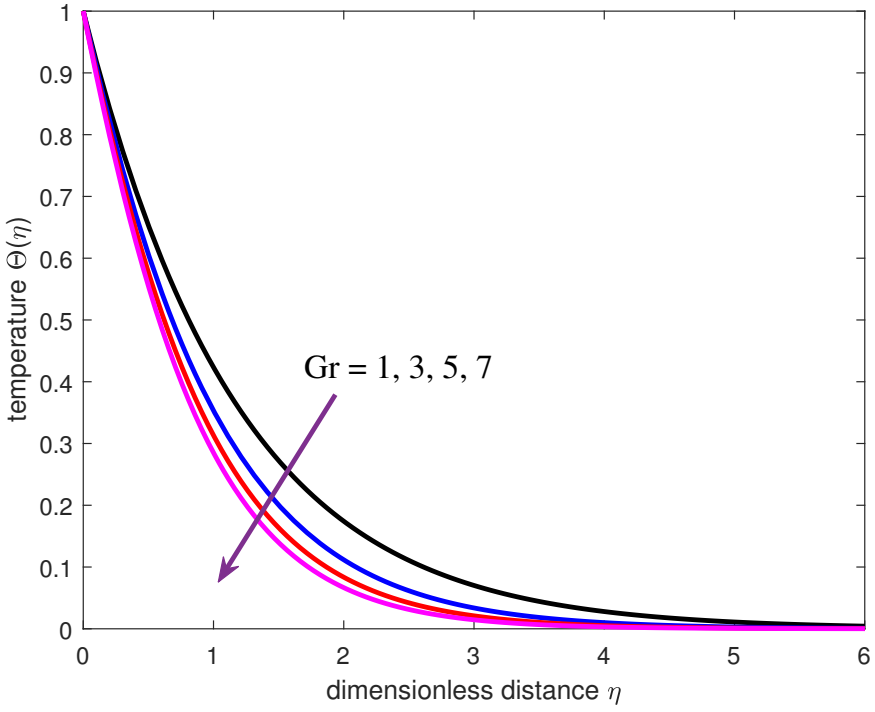

Figure 4.8: Temperature with Grashof number

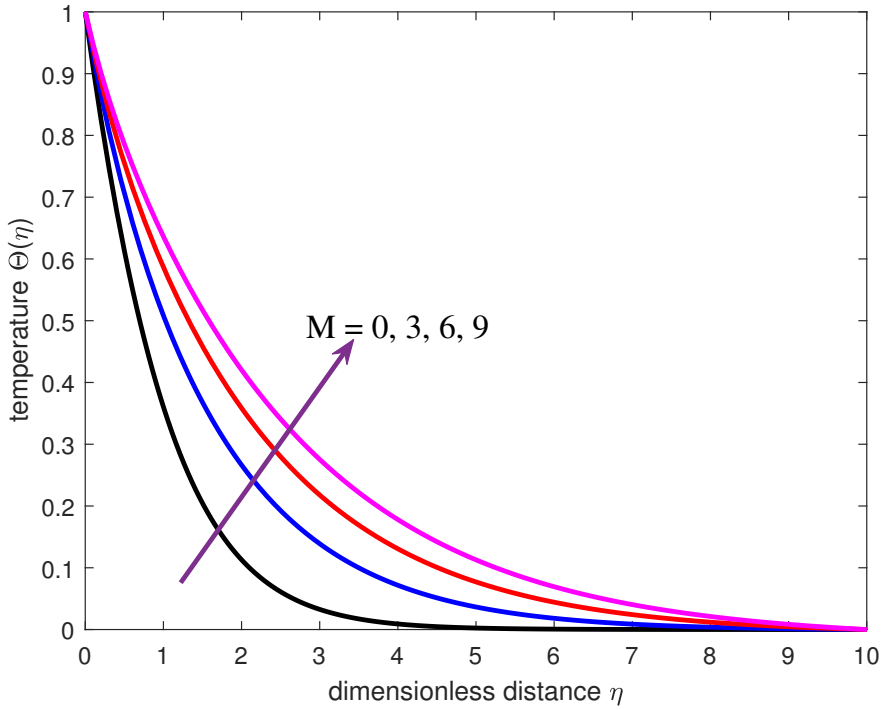

Figure 4.9: Temperature with Magnetic parameter

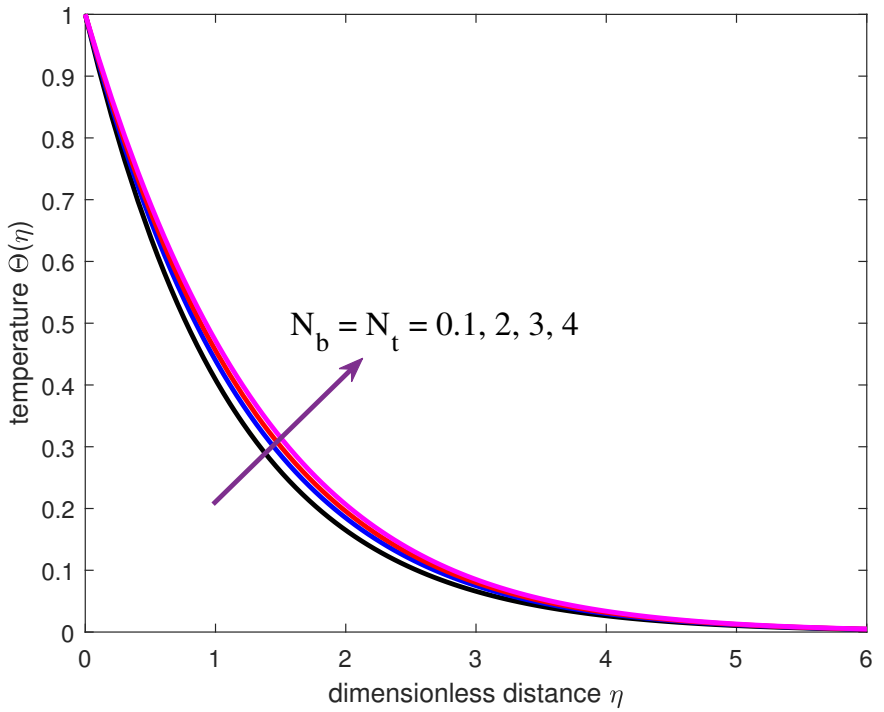

Figure 4.10: Temperature with Brownian motion parameter and Thermophoretic parameter

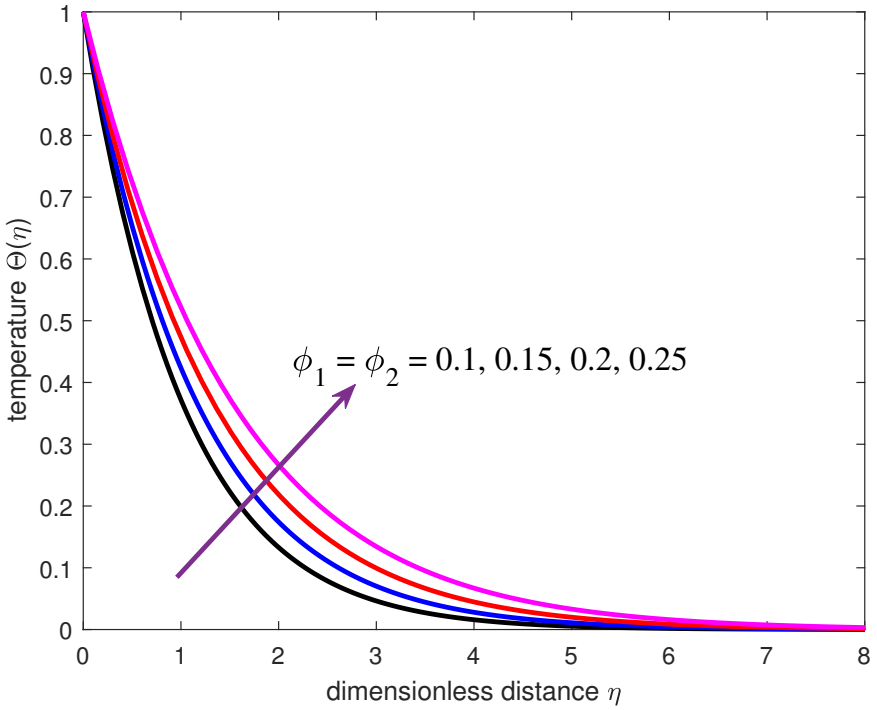

Figure 4.11: Temperature with volume fraction

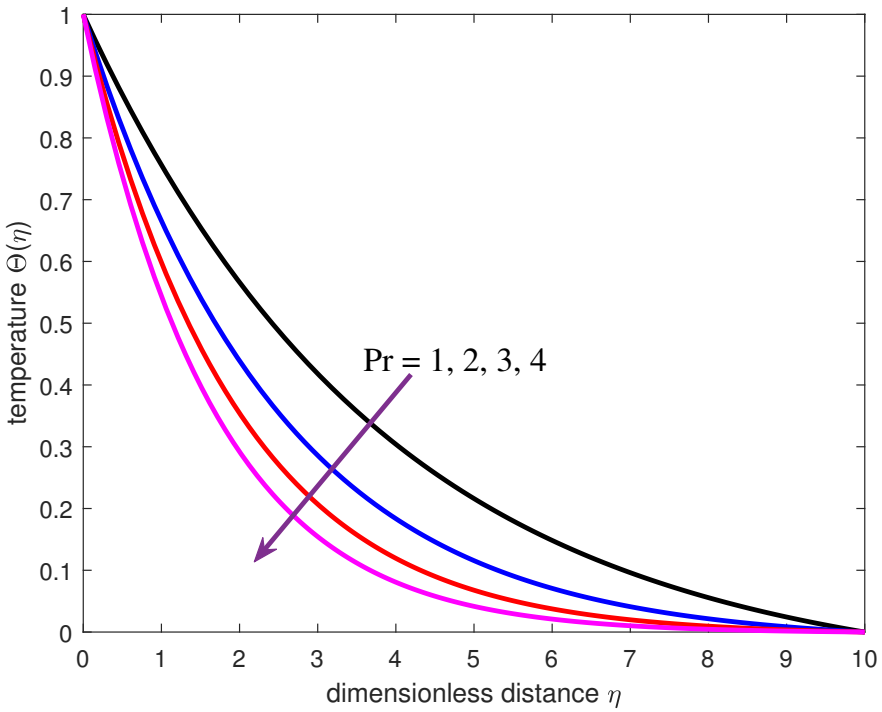

Figure 4.12: Temperature with Prandtl number

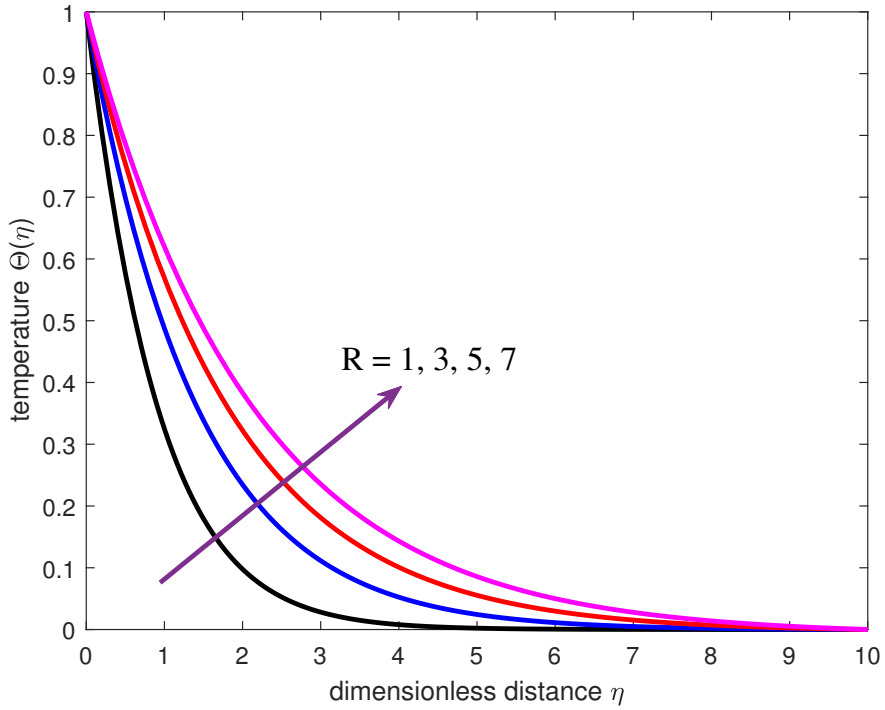

Figure 4.13: Temperature with Radiation parameter

4.3 Concentration profile

Figures (4.14 - 4.19) illustrate the effects of the flow parameters on the concentration. As the Casson parameter γ increases, the concentration at the boundary layer increases. Consequently, the concentration profile increases as the Casson parameter increases (as shown in figure (4.14)). In figure (4.15), the concentration profile decreases with increasing Grashof number. An increase in the Grashof number implies an increase in buoyancy. Buoyancy makes the particles unable to settle at the boundary layer and therefore enhances the particle migration from the boundary layer. Hence, a decrease in the concentration profiles is observed as the Grashof number increases. Figure (4.16) shows the concentration profile increases with increasing Magnetic parameter. Increasing the Magnetic parameter generates the Lorentz force which results in the thickening of the momentum boundary layer. This directly translates to the increase experienced in the concentration profile. Figure

(4.17) shows that simultaneously increasing the Brownian motion and the thermophoretic parameters reduce the concentration profiles at the boundary layer. The Brownian motion and thermophoretic parameters measure how rapidly the fluid particles migrate from the boundary layer and within the flow. Increasing both Brownian and thermophoretic parameters enhances the migration of fluid particles from the boundary layer and therefore reduces the amount of nanoparticles in the boundary layer. This in turn reduces the concentration profile as the Brownian motion and the Thermophoretic parameters are increased. Figure (4.18) shows that concentration profiles increase with an increase in Prandtl number. Increasing the Prandtl number results in the thickening of the momentum boundary layer and thereby increases concentration profiles. In figure (4.19), increasing the Radiation parameter results in a decrease in the concentration profile. This is because, as the Radiation parameter increases, heat is generated in the flow. A surge in the flow temperature enhances the migration of nanoparticles from the boundary layer and consequently reduces the particle concentration at the boundary layer. This results in a decrease in the momentum boundary layer which translates to a decrease in the concentration profiles.

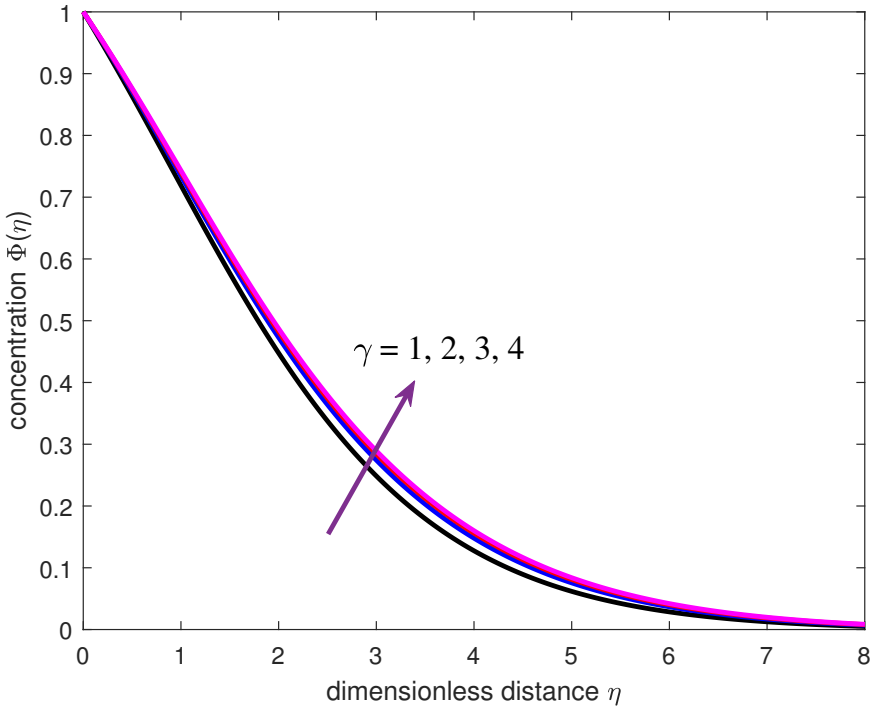

Figure 4.14: Concentration with Casson parameter

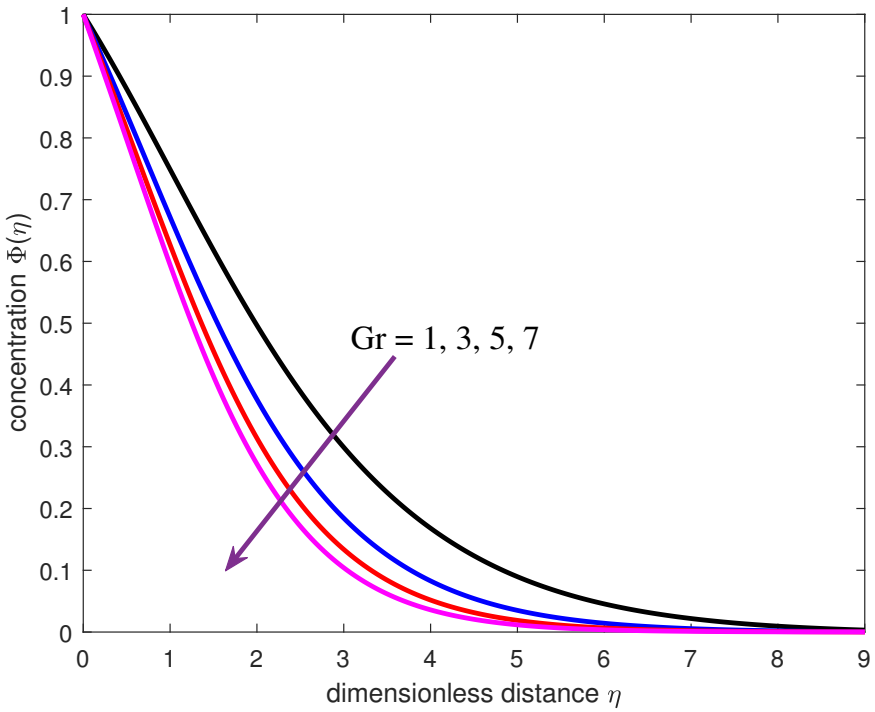

Figure 4.15: Concentration with Grashof number

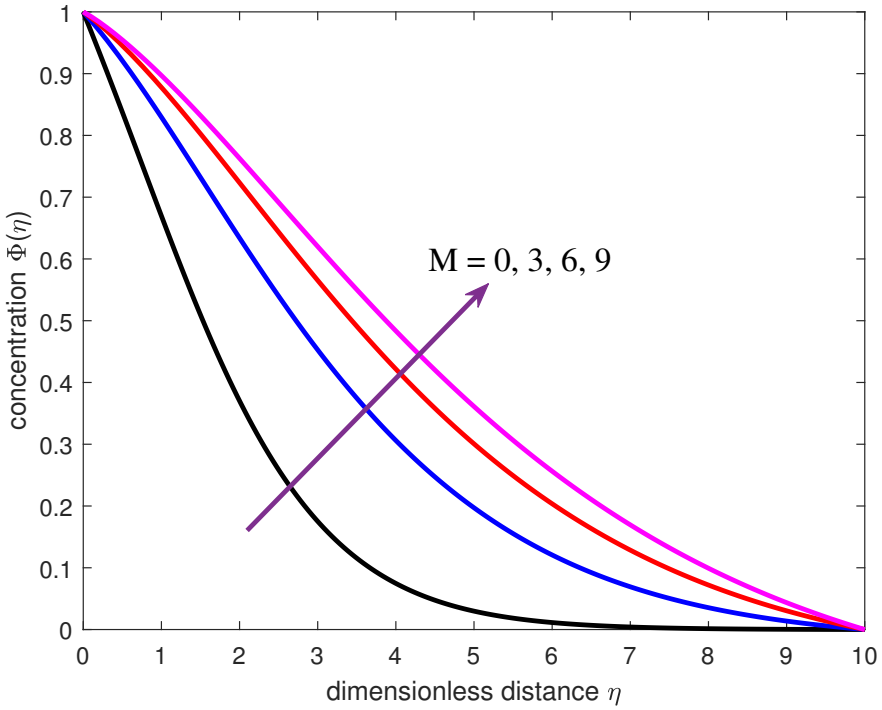

Figure 4.16: Concentration with Magnetic parameter

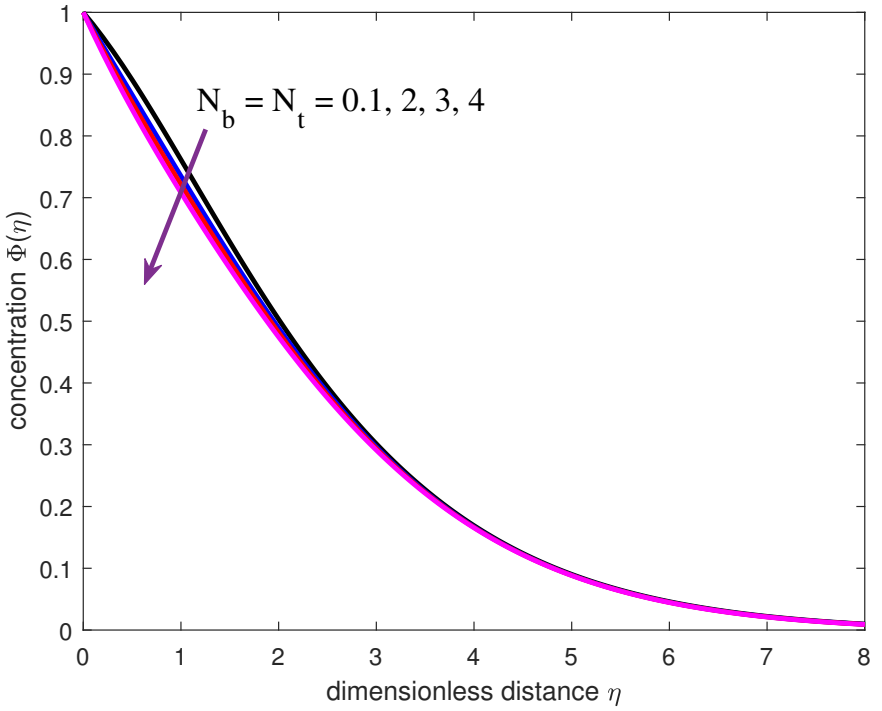

Figure 4.17: Concentration with Brownian motion parameter

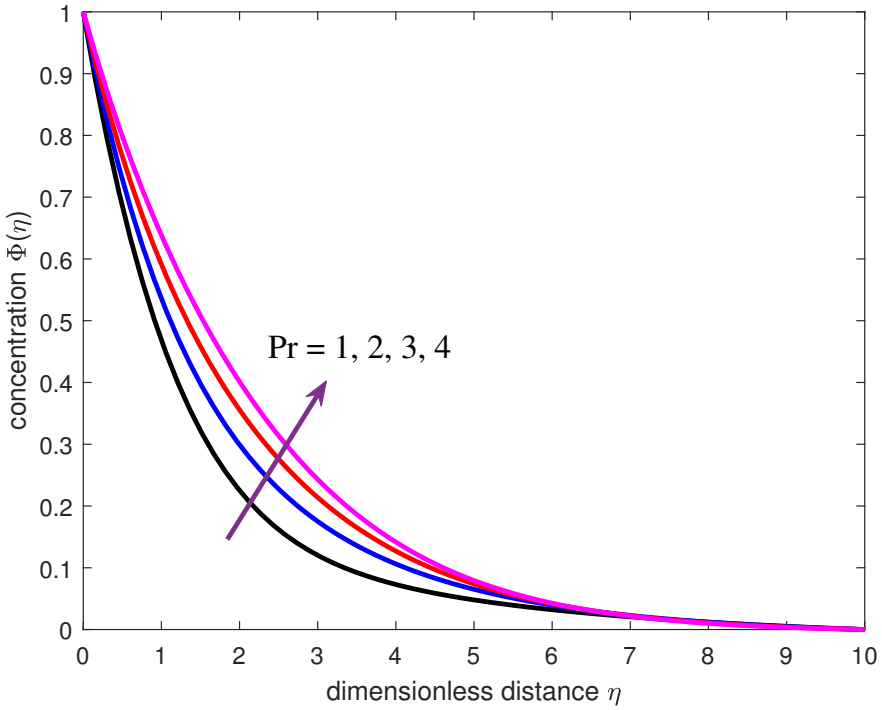

Figure 4.18: Concentration with Prandtl number

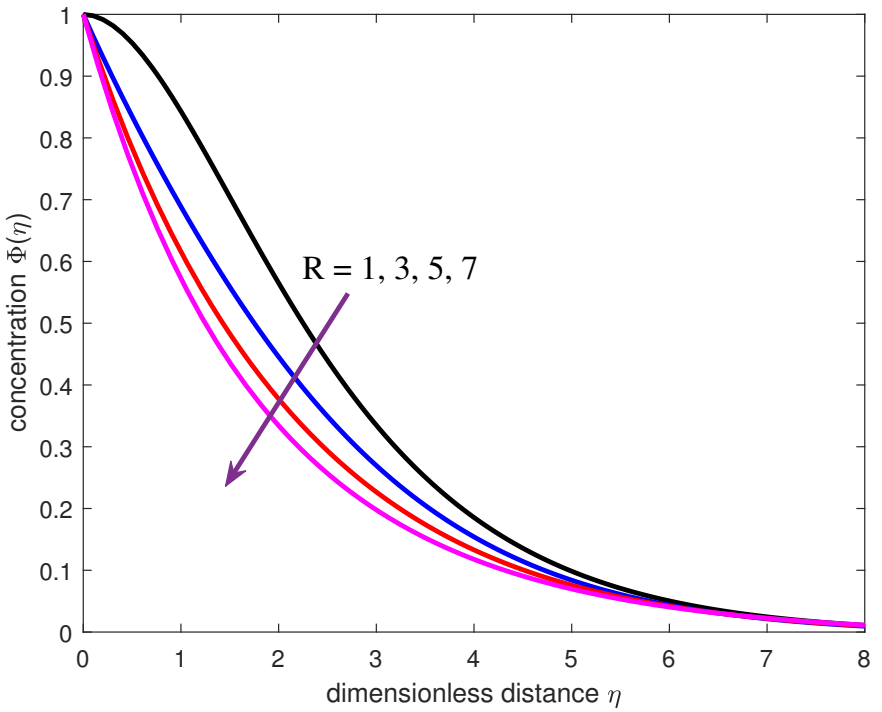

Figure 4.19: Concentration with Radiation parameter

4.4 Quantities of Interest

The Skin friction coefficient, Sherwood number, and Nusselt number are computed and shown in table (4.2). The skin friction coefficient represents the drag experienced at the wall due to viscosity, the Sherwood number measures the mass transfer rate while the Nusselt number measures the heat transfer rate. It is clear that Skin friction coefficient, Sherwood number, and Nusselt number increase with increasing Grashof number while they all decrease with increasing magnetic field. Increasing Casson fluid parameter causes an increase in the skin friction but reduces both heat transfer rate and mass transfer rate. By increasing the Prandtl number, skin friction coefficient and mass transfer rate decline but the heat transfer rate is enhanced. The radiation parameter causes a rise in the skin friction coefficient and mass transfer rate but a decline in heat transfer rate.

Gr	M	γ	Pr	R	$Re^{1/2}C_f$		$Re^{-1/2}N_u$		$Re^{-1/2}Sh$	
0.5	1	10	7.2	2	-1.245633315	↑	0.817985874	↑	0.175714756	↑
2					-0.581040882		0.917571328		0.263425671	
3.5					0.013917089		0.980956426		0.312889511	
5					0.569252613		1.029835214		0.348744744	
1	0.5				-0.770475997	↓	0.89768154	↓	0.251527008	↓
	2				-1.416580567		0.794891068		0.160088346	
	3.5				-1.904957996		0.721866343		0.113210799	
	5				-2.310164241		0.666172034		0.087029664	
	1	0.5			-1.878560408	↑	0.914037518	↓	0.273490546	↓
		2			-1.226410213		0.875955507		0.229718612	
		3.5			-1.11489622		0.867363509		0.22127766	
		5			-1.068341673		0.863537079		0.217717838	
		10	0.5		-0.798933832	↓	0.195647542	↑	0.81439048	↓
			2		-0.880842247		0.407504098		0.642261504	
			3.5		-0.931761986		0.562481803		0.500400584	
			5		-0.969721143		0.692952712		0.375550069	
			7.2	0.5	-1.104480262	↑	1.299137965	↓	-0.22112938	↑
				2	-1.012422753		0.858737594		0.213431548	
				3.5	-0.965114487		0.680157903		0.388498895	
				5	-0.934952758		0.578255755		0.486205056	

Table 4.2: Quantities of Engineering Interests evaluated at $N_b = 1; N_t = 1; Sc = 0.63; \phi_1 = \phi_2 = 0.15$

Chapter 5

Conclusion and Recommendation

5.1 Conclusion

This study analyses the magnetohydrodynamics of HAMT rate in SWCNT-Graphene Casson hybrid nanofluid over an ESS. The system of PDEs that model the flow [equation (3.1.1) to equation (3.1.4)], and the boundary conditions [equation (3.1.5) to equation (3.1.6)], are formulated and used for studying the HAMT rate of a hybrid Casson nanofluid. Suitable similarity variables stated in equation (3.2.1) are used to remove dimensions from the model and a dimensionless form of the model is obtained as equation (3.2.10) with the dimensionless boundary conditions given as equation (3.2.11). The model is then rewritten as a system of ODEs from equation (3.2.12) to equation (3.2.18) with the conditions from equation (3.4.1) to equation (3.4.2). The effects of parameters like Casson, Grashof number, Magnetic Brownian motion, Thermophoretic, Prandtl number and Radiation, on the flow velocity, temperature, and concentration are presented in form of graphs and tables [figure (4.1) to figure (4.19) and table (4.1) to table (4.2)] . The resulting graphs and tables are analysed and discussed. The results show that when the parameters are increased;

1. The primary flow velocity decreases with Casson fluid parameter, Prandtl number, and Magnetic parameter, but increases with Grashof number, Radiation parameter, and with the simultaneous increase in Brownian motion parameter. and Thermophoretic parameter.

2. The temperature profiles increase with Casson parameter, Magnetic parameter, Volume fraction, Radiation parameter, the simultaneous increase in the

Brownian motion parameter, and thermophoretic parameter, but decrease with Grashof number and Prandtl number.

3. The concentration profiles experience an increase with Casson parameter, Magnetic parameter, Prandtl number, but a decrease with Grashof number, Radiation parameter, and with the simultaneous increase of the Brownian motion parameter and the thermophoretic boundary parameter.

4. The Skin friction coefficient increases with the Grashof number, Casson fluid parameter, and radiation parameter but decreases with magnetic field strength and Prandtl number.

5. Nusselt number increases with Grashof number and Prandtl number but decreases with Casson fluid parameter, magnetic field strength, and radiation parameter.

6. Sherwood number increases with Grashof number and radiation parameter but decreases with Casson fluid parameter, magnetic field strength, and Prandtl number.

Therefore, the conclusions that follow can be drawn from the study results:

1. To achieve a reduction in the surface drag, the magnetic field strength should be increased.

2. To increase heat transfer rate, the Prandtl number and buoyancy should be increased

3. To increase mass transfer rate, thermal radiation should be increased.

4. Flow velocity can be increased by increasing thermal radiation and buoyancy.

5.2 Recommendations

This study investigates HAMT rate in the magnetohydrodynamic flow of SWCNT-Graphene Casson hybrid nanofluid over a surface which is stretching exponentially. Further research can be carried out as extensions of this current study. The following modifications to the current study are recommended to be carried out;

1. The study can be extended to the unsteady fluid flow case.
2. The stretching of the surface can be considered as sinusoidal rather than exponential, as the case is in many industries.

References

Alfvén, H. (1942). Existence of Electromagnetic-Hydrodynamic Waves. *Nature*, 150(3805):405–406.

Babar, H. and Ali, H. M. (2019). Towards hybrid nanofluids: Preparation, thermophysical properties, applications, and challenges. *Journal of Molecular Liquids*, 281:598–633.

Bhattad, A. and Sarkar, J. (2019). Effects of nanoparticle shape and size on the thermohydraulic performance of plate evaporator using hybrid nanofluids. *Journal of Thermal Analysis and Calorimetry*, 143(1):767–779.

Bibi, S., Elahi, Z., and Shahzad, A. (2020). Impacts of different shapes of nanoparticles on silicon dioxide nanofluid flow and heat transfer in a liquid film over a stretching sheet. *Physica Scripta*, 95(11):115217.

Bilal, M., Arshad, H., Ramzan, M., Shah, Z., and Kumam, P. (2021). Unsteady hybrid-nanofluid flow comprising ferrousoxide and CNTs through porous horizontal channel with dilating/squeezing walls. *Scientific Reports*, 11(1):12637.

Blair, G. W. S. (1959). An equation for the flow of blood, plasma and serum through glass capillaries. *Nature*, 183(4661):613–614.

Choi, U. S. and Eastman, J. (1995). Enhancing Thermal Conductivity of Fluids with Nanoparticles. *ASME International Mechanical Congress and Exposition, San Francisco*, (12–17).

Ekiciler, R., Çetinkaya, M. S. A., and Arslan, K. (2020). Effect of shape of nanoparticle on heat transfer and entropy generation of nanofluid-jet impingement cooling. *International Journal of Green Energy*, 17(10):555–567.

Elias, M., Miqdad, M., Mahbubul, I., Saidur, R., Kamalisarvestani, M., Sohel, M., Hepbasli, A., Rahim, N., and Amalina, M. (2013). Effect of nanoparticle shape on the heat transfer and thermodynamic performance of a shell and tube heat exchanger. *International Communications in Heat and Mass Transfer*, 44:93–99.

Hayat, T. and Nadeem, S. (2017). Heat transfer enhancement with ag–CuO/water hybrid nanofluid. 7:2317–2324.

Huminic, G. and Huminic, A. (2018). Hybrid nanofluids for heat transfer applications – a state-of-the-art review. *International Journal of Heat and Mass Transfer*, 125(12):82–103.

Hussain, S. M., Sharma, R., Mishra, M. R., and Alrashidy, S. S. (2020). Hydromagnetic Dissipative and Radiative Graphene Maxwell Nanofluid Flow Past a Stretched Sheet-Numerical and Statistical Analysis. *Mathematics*, 8(11).

Jiang, Y., Zhou, X., and Wang, Y. (2019). Effects of nanoparticle shapes on heat and mass transfer of nanofluid thermocapillary convection around a gas bubble. *Microgravity Science and Technology*, 32(2):167–177.

Juma, B. A., Oke, A. S., Mutuku, W. N., Ariwayo, A. G., and Ouru, O. J. (2022). Dynamics of williamson fluid over an inclined surface subject to coriolis and lorentz forces. *Engineering and Applied Science Letter*, 5(1):37–46.

Kigio, J. K., Nduku, M. W., and Samuel, O. A. (2021). Analysis of volume fraction and convective heat transfer on MHD casson nanofluid over a vertical plate. *Fluid Mechanics*, 7(1):1.

Maxwell, J. C. (1873). A Treatise on Electricity and Magnetism. *Nature*, 7:478–480.

Nahirnyak, V. M., Yoon, S. W., and Holland, C. K. (2006). Acousto-mechanical and thermal properties of clotted blood. *The Journal of the Acoustical Society of America*, 119(6):3766–3772.

Nandeppanavar, M. M., Kemparaju, M., and Raveendra, N. (2022). Effect of richardson number on double-diffusive mixed convective slip flow, heat and mass transfer of MHD casson fluid. *Proceedings of the Institution of Mechanical Engineers, Part E: Journal of Process Mechanical Engineering*, 236(5):1958–1966.

Oke, A., Animasaun, I., Mutuku, W., Kimathi, M., Shah, N. A., and Saleem, S. (2021). Significance of coriolis force, volume fraction, and heat source/sink on the dynamics of water conveying 47 nm alumina nanoparticles over a uniform surface. *Chinese Journal of Physics*, 71:716–727.

Oke, A. S., Fatunmbi, E. O., Animasaun, I. L., and Juma, B. A. (2022). Exploration of ternary-hybrid nanofluid experiencing coriolis and lorentz forces: case of three-dimensional flow of water conveying carbon nanotubes, graphene, and alumina nanoparticles. *Waves in Random and Complex Media*, pages 1–20.

Othman, M. N., Jedi, A., and Bakar, N. A. A. (2021). MHD flow and heat transfer of hybrid nanofluid over an exponentially shrinking surface with heat source/sink. 11(17):8199.

Pathak, S. K., Kumar, R., Goel, V., Pandey, A., and Tyagi, V. (2022). Recent advancements in thermal performance of nano-fluids charged heat pipes used for thermal management applications: A comprehensive review. *Applied Thermal Engineering*, 216:119023.

Roy, N. C. and Pop, I. (2022). Heat and mass transfer of a hybrid nanofluid flow with binary chemical reaction over a permeable shrinking surface. *Chinese Journal of Physics*, 76:283–298.

Sheikholeslami, M., Mehryan, S., Shafee, A., and Sheremet, M. A. (2019). Variable magnetic forces impact on magnetizable hybrid nanofluid heat transfer through a circular cavity. 277:388–396.

Subhani, M. and Nadeem, S. (2018). Numerical analysis of micropolar hybrid nanofluid. 9(4):447–459.

Suresh, S., Venkitaraj, K., Selvakumar, P., and Chandrasekar, M. (2011). Synthesis of al2o3–cu/water hybrid nanofluids using two step method and its thermo physical properties. 388(1-3):41–48.

Takhar, H., Chamkha, A., and Nath, G. (2000). Flow and mass transfer on a stretching sheet with a magnetic field and chemically reactive species. *International Journal of Engineering Science*, 38(12):1303–1314.

Tassaddiq, A., Khan, S., Bilal, M., Gul, T., Mukhtar, S., Shah, Z., and Bonyah, E. (2020). Heat and mass transfer together with hybrid nanofluid flow over a rotating disk. 10(5):055317.

Venkatesan, J., Sankar, D. S., Hemalatha, K., and Yatim, Y. (2013). Mathematical analysis of casson fluid model for blood rheology in stenosed narrow arteries. *Journal of Applied Mathematics*, 2013:1–11.

Waini, I., Ishak, A., and Pop, I. (2019). Unsteady flow and heat transfer past a stretching/shrinking sheet in a hybrid nanofluid. 136:288–297.

Wang, X. and Mujumdar, A. S. (2008). (a review on nanofluids- part 1: Theoretical and numerical investigations). *Brazillian Journal of Chemical Engineering*, 25(4):613–630.

Zainal, N. A., Nazar, R., Naganthran, K., and Pop, I. (2020). MHD flow and heat transfer of hybrid nanofluid over a permeable moving surface in the presence of thermal radiation. 31(3):858–879.

Appendix I: Plan of Work

S/N	WORK DESCRIPTION	DURATION
1.	Literature review, proposal writing and defence	3 months
2.	Proposal corrections	1 month
3.	Project writing	4 months

Appendix II: Budget

S/N	ITEMS	COST (KSh)
1.	Publishing Journal	30,000.00
2.	Internet Services	30,000.00
3.	Typing, Printing, Photocopies and Binding	30,000.00
4.	Attending Conferences	50,000.00
5.	Laptop	60,000.00
6.	Miscellaneous Expenses	50,000.00
	TOTAL	250,000.00

MATLAB CODES

```
function res = BC(u0,uinf)
res = [u0(1)
                u0(2)-1
                u0(4)-1
                u0(6)-1
                uinf(2)
        uinf(4)
        uinf(6)];
end

global Gr M gam A1 Nb Nt Pr A2 R Sc
Gr =1; M=1; gam=10; Nb=1; Nt=1; Pr=7; R=2; Sc=0.63;
phi_1 = 0.15; phi_2 = 0.15; phi = phi_1 + phi_2;
% CNTs SOURCE: doi: 10.1038/s41598-021-91188-1
%Graphene SOURCE: doi: 10.3390/math8111929
% Blood SOURCE: doi: 10.1121/1.2201251
rho_1 = 2600; cp_1=425; k_1=6600; % SWCNT
%rho_1 = 1600; cp_1=796; k_1=3000; % MWCNT
rho_2=2250; cp_2=2100; k_2=2500; %Graphene
rho_f=1093; cp_f=3210; k_f=0.451; %Blood
A1=(1-phi)^(-5/2)/(1-phi+(phi_1*rho_1+phi_2*rho_2)/rho_f);
B1 = (1+2*phi)*(phi_1*k_1 + phi_2*k_2) + 2*(1-phi)*phi*k_f;
B2 = (1-phi)*(phi_1*k_1 + phi_2*k_2) + (2+phi)*phi*k_f;
B3 = 1-phi+(phi_1*rho_1*cp_1 + phi_2*rho_2*cp_2)/(rho_f*cp_f);
A2=B1/(B2*B3); sol_dir = [0 0 0 0 0 0 0]; time_span = linspace(0,10,100);
Par_Val = 'M = 1; \gamma = 10; N_b = 1; N_t = 1; Pr = 7;';
```

```
Par_Val = strcat(Par_Val,' R = 2; Sc = 0.63; \phi_1 = 0.15; \phi_2 = 0.15
Values = 'Sc =  '; i=1;
for Sc=[1,2,3,4]
    txt = 'Sc'; Values = strcat(Values,string(Sc),'; ');
     dim_1 = [.7 .3 0.1 .1]; dim_2 = [.4 .5 0.5 .15];
    solver_data = bvpinit(time_span, sol_dir);
    sol = bvp4c(@ODEfun, @BC, solver_data);
    if i==1
        Line_style = 'k-';
    elseif i==2
        Line_style = 'b-';
    elseif i==3
        Line_style = 'r-';
    elseif i==4
        Line_style = 'm-';
    end
        if i~=4
        figure(2), plot(sol.x,sol.y(2,:), Line_style,'LineWidth',2)
        xlabel('dimensionless distance \eta'), ylabel("velocity f'(\eta)"
        hold on
                figure(4), plot(sol.x,sol.y(4,:), Line_style,'LineWidth',
        xlabel('dimensionless distance \eta'), ylabel("temperature \Theta
        hold on
        figure(6), plot(sol.x,sol.y(6,:), Line_style,'LineWidth',2)
        xlabel('dimensionless distance \eta'), ylabel("concentration \Phi
        hold on
        i=i+1;
    else
        figure(2), plot(sol.x,sol.y(2,:), Line_style,'LineWidth',2)
```

```
        xlabel('dimensionless distance \eta'), ylabel("velocity f'(\eta)"
        annotation('textbox',dim_1,'String',Values);
        annotation('textbox',dim_2,'String',Par_Val);
        hold on
        txt_vel = strcat(txt,'_Vel'); saveas(gcf,txt_vel)
        figure(4), plot(sol.x,sol.y(4,:), Line_style,'LineWidth',2)
        xlabel('dimensionless distance \eta'), ylabel("temperature \Theta
        annotation('textbox',dim_1,'String',Values);
        annotation('textbox',dim_2,'String',Par_Val);
        hold on
        txt_temp = strcat(txt,'_Temp'); saveas(gcf,txt_temp)
        figure(6), plot(sol.x,sol.y(6,:), Line_style,'LineWidth',2)
        xlabel('dimensionless distance \eta'), ylabel("concentration \Phi
        annotation('textbox',dim_1,'String',Values);
        annotation('textbox',dim_2,'String',Par_Val);
        hold on
        txt_conc = strcat(txt,'_Conc'); saveas(gcf,txt_conc)
        i=i+1;
    end
end

function dudt = ODEfun(eta,u)
    global Gr M gam A1 Nb Nt Pr A2 R Sc
        du1 = u(2);   du2 = u(3);
    du3 = -(2*Gr*u(4) - 2*M*u(2) - 2*u(2)^2 + u(1)*u(3))/((1+(1/gam))*A1)
    du4 = u(5); du5 = -(Nb*u(5)*u(7) + Nt*u(5)^2 - Pr*u(4)*u(2) + Pr*u(5)
    du6 = u(7); du7 = -(Nt*du5/Nb + Sc*u(1)*u(7) - Sc*u(2)*u(6));
dudt = [du1; du2; du3; du4; du5; du6; du7];
end
```